Situating the salience and parietal memory networks in the context of multiple parallel distributed networks using precision functional mapping

Authors: Young Hye Kwon[1,10*], Joseph J. Salvo[1], Nathan L. Anderson[1], Donnisa Edmonds[1], Ania M. Holubecki[1], Maya Lakshman[1], Kwangsun Yoo[2,3], B.T. Thomas Yeo[4], Kendrick Kay[5], Caterina Gratton[6,7,8,9], Rodrigo M. Braga[1,7*]

Affiliations: [1] Department of Neurology, Northwestern University, Chicago, IL, 60611, USA.
[2] Department of Digital Health, Samsung Advanced Institute for Health Sciences and Technology, Sungkyunkwan University, Seoul, 06351, Republic of Korea.
[3] AI Research Center, Research Institute for Future Medicine, Samsung Medical Center, Seoul, 06351, Republic of Korea.
[4] Centre for Sleep & Cognition, Centre for Translational MR Research and Department of Electrical & Computer Engineering, National University of Singapore, 117549, Singapore.
[5] Center for Magnetic Resonance Research (CMRR), Department of Radiology, University of Minnesota, Minneapolis, MN, 55455, USA.
[6] Department of Psychology, Florida State University, Tallahassee, FL, 32306, USA.
[7] Department of Psychology, Northwestern University, Evanston, IL, 60208, USA.
[8] Department of Psychology, University of Illinois Urbana-Champaign, Champaign, IL, 61820, USA.
[9] Beckman Institute for Advanced Science and Technology, University of Illinois Urbana-Champaign, Urbana, IL, 61801, USA.
[10] Lead contact

***Corresponding Authors:** Young Hye Kwon (younghye.kwon@northwestern.edu) and Rodrigo M. Braga (rbraga@nortwestern.edu)

Summary

Brain networks serving higher cognitive functions are widely distributed across frontal and posterior association zones. Two exceptions have been the parietal memory (PMN) and salience networks (SAL), which are typically restricted to posterior (e.g., posterior cingulate and lateral parietal cortex) and anterior (medial prefrontal and anterior insular cortex) areas, respectively. Using high-resolution neuroimaging, we show that individualized estimates of the PMN extend beyond the posterior set and encompass frontal and insula regions canonically ascribed to SAL. This suggests that SAL and PMN form a unified 'SAL/PMN' network. Task-based analyses confirm that both anterior and posterior components of SAL/PMN show recognition-related activity. Comparison of 3T and 7T data suggests that high-resolution data more readily revealed the unified network, underscoring the importance of fine-scale distinctions for veridical representation of brain networks. Importantly, the unified network better matches the expected parallel distributed network organization that is characteristic of association cortex.

Introduction

The cerebral cortices comprise large-scale networks that are specialized for different cognitive functions.[1,2,3,4,5] Knowledge of the detailed anatomy of the networks, including the

constituent regions and how these fit within broader topographical patterns, can provide clues to the component processes of cognition and their anatomical bases (e.g.,[6,7,8]). One example is recognition,[9] a type of declarative memory that is commonly divided into processes of recollection (i.e., the mental re-experiencing of a previous experience) and familiarity (i.e., the subjective feeling that something has been previously experienced[10,11,12]). Although these processes likely interact during recognition, evidence from functional brain imaging supports that distinct brain systems are associated with recollection and familiarity (e.g.,[10,13,14]).

Tasks targeting recollection often reveal increased activity in a broad network that includes regions within the canonical 'default network' or 'DN'.[15,16,17,18] The implicated network is widely distributed, including regions at or near the posterior cingulate, posterior inferior parietal, lateral temporal, medial and lateral prefrontal, and parahippocampal cortices.[16,19] This network shows increased activity when participants are asked to think about a past or prospective future event,[15] and is robustly activated when mental scenes are contemplated.[20,21,22] In contrast, tasks that target familiarity, such as those involving detection of previously seen images, typically reveal activity in a much more restricted posteromedial set of regions, a network sometimes called the 'parietal memory network' or 'PMN'.[23,24] The PMN includes a region at or near the precuneus (PCU) and a separate region in the rostral posterior cingulate cortex (rPCC) within the callosal sulcus. These PMN regions surround the posteromedial regions of the canonical DN,[1,3,5] which forms a key identifying feature of the PMN. Functionally, the PMN shows increased activity to previously seen stimuli – the so-called 'repetition enhancement effect'[25, 26] – even in the absence of an explicit requirement for the stimuli to be identified as familiar[24] (see also[27]). Hence, evidence supports that two distinct networks, one within canonical DN regions and one being the PMN, play complementary but dissociable roles in recognition.

The DN is a widely distributed network, containing regions in multiple association areas; an organizational motif that is characteristic of association cortex.[2,8] In contrast, the PMN is typically restricted to posteromedial cortex (i.e., the PCU and rPCC) and, sometimes, lateral parietal cortex. This bears scrutiny given that the PMN is also located deep within association zones, suggesting the PMN should also have a distributed network organization that more resembles the DN and other association networks (e.g., see[28, 29]). Another exception is the salience network (SAL), which typically comprises regions within the anterior cingulate and medial prefrontal cortex (collectively referred to as 'mPFC' here) and anterior insula (aINS), and sometimes the rostrolateral prefrontal cortex (rPFC). SAL also appears to break the expected parallel distributed pattern of association networks, but in this case by being restricted to anterior cortices, while PMN is confined to posterior cortices. These discrepancies raise the possibility that SAL and PMN are anterior and posterior components of a larger unified system that fits the distributed network motif.[30,31,32] Of note, the putative functions of the SAL network in responding to relevant stimuli[33] are likely integral to the detection of novel or familiar stimuli in tasks typically used to define the PMN.[23,24]

There have been conflicting accounts regarding which regions comprise the PMN (as reviewed in[34]). Some functional connectivity (FC) estimates restrict the PMN to the core PCU and rPCC regions, particularly when winner-takes-all algorithms are used (e.g., compare the 13th and 34th figures in the Yeo et al.[5]; see also[1,3,35]), but several studies have identified additional PMN regions. A PMN region is often reported in the inferior parietal lobule (IPL), sometimes at or near the posterior angular gyrus (e.g.,[23,34,36]) or sometimes in a more anterior location within the intraparietal sulcus.[24,37,38,39] Less frequently, the PMN has been reported to include frontal regions at or near the rPFC[25,40,41,42] and mPFC, which are more commonly reported in task-based analyses[40,41,42] than FC estimates, which led to the proposal that the frontal regions are part of a separate network that is recruited alongside the PMN in certain task contexts (e.g., see[43]). However, Gordon et al.[37] showed that some individuals do display frontal PMN regions in task-free FC estimates when individual differences are specifically considered. In their analysis, some individuals showed a further PMN region at or near the ramus marginalis of the cingulate sulcus (RMC). In summary, data support that the PMN may include multiple regions beyond the posteromedial set (i.e., the PCU, rPCC, IPL, rPFC, mPFC, RMC), but emphasize that considerable individual differences may have led to these regions being missed in group-level estimates.[34] Notably, the putative anterior PMN regions are typically situated at or near components of SAL.

Recently, advances in functional magnetic resonance imaging (fMRI) have allowed the estimation of brain networks reliably within the individual through repeated scanning.[44,45] The individual-level maps capture idiosyncratic details of the networks present in each individual,[28,37,44,46] revealing new insights (e.g.,[17,28,29,36,46,47,48,49,50,51]). Zheng et al.[51] analyzed extensively collected data from 10 individuals and found that, while all individuals displayed a PMN that included the core PCU and rPCC regions, the other, additional regions were only observed in some individuals (see also Gordon et al.[37]). Recently, using a multi-level Bayesian parcellation that incorporates information about individual variability to stabilize network estimation, Kong et al.[38] defined the PMN as a widely distributed network, including regions in a total of 7 distinct cortical zones, including PCU, rPCC, RMC, rPFC, IPL and mPFC, as well as aINS; see 'Control C' network in[38]). The aINS regions of PMN, while surprising, were also present in 2 individuals in the analysis by Gordon et al.[37], upon close inspection. These prior accounts show that even when more powerful individual-level analyses are deployed, the detection of PMN regions beyond the posteromedial set has been inconsistent.

Although individuals might truly vary in the number of brain regions connected to the PMN, a simpler explanation is that small regions may have been missed in some individuals because they fall below the signal limits of the imaging procedures used. We hypothesized that high-resolution 7T network estimation within individuals would resolve multiple PMN regions beyond the posteromedial set consistently, including in regions that are difficult to resolve such as the insula.[63]

Results

High-resolution fMRI reveals that the PMN is distributed across multiple cortical zones

Temporal signal-to-noise ratio (tSNR) maps revealed high average tSNR in each individual (Table S1), despite the small voxel size (1.8 mm isotropic; see Supp. Fig. S1). Runs passing quality control were divided into discovery and validation (i.e., replication and triplication) datasets in each individual. We initially explored the discovery dataset, and then performed hypothesis-testing analyses in the validation datasets, before replicating and triplicating network maps in the validation datasets.

On initial exploration of functional connectivity patterns in one of the NSD subjects, the observation was made that a network resembling the PMN could be defined by selecting seed regions from the posteromedial cortex. The estimated network highlighted the PCU and rPCC regions[3,5,23] but also included multiple lateral and frontal cortical regions that showed high correlations (r ~ 0.6; Fig. 1). Hints of a further region were also observed in the lateral temporal cortex (LTC; explored later) which typically suffers from signal dropout in fMRI. Motivated by this, we explored the organization of this network in other individuals and using multiple approaches. First, we manually selected seed vertices from the rPFC in each individual (Fig. 1A, first column) whose correlation maps also contained the core PMN regions in the PCU and rPCC. A single "best" PMN seed was then selected for each participant by visually comparing the correlation maps in the discovery dataset, emphasizing strong correlation values throughout the network. In each participant, the PMN appeared as a distributed network with regions in multiple cortical association zones.

Seeds were initially selected from the rPFC (Fig. 1), following[28,46,47]. The distributed organization of the network was confirmed by selecting seeds in five cortical zones (Fig. 2 and Supp. Fig. S2), demonstrating that the regions formed an interconnected distributed network through multiple seeds, including in regions underemphasized in the literature such as the aINS and mPFC.

We next defined other networks in the proximity of the PMN to ensure that the estimated PMN was not being conflated with other networks. In each participant, we defined multiple networks (including DN-A, DN-B, FPN-A, and FPN-B) using seeds in the lateral prefrontal cortex, none of which showed connections to the characteristic posteromedial set of PMN regions, confirming our estimate of the PMN was a distinct network (Supp. Figs. S3, S5—S8). These analyses also revealed two parallel distributed networks within canonical CON regions (which we refer to as CON-A and CON-B; see also[38]).

Once all networks had been defined using a manual seed-based approach, we performed data-driven clustering[38] to define multiple networks simultaneously (Fig. 1). The estimates shown in Fig. 1 were consistent across multiple levels of clustering (explored later). These analyses confirmed through multiple approaches that when defined in individuals using high-resolution data, the PMN is a widely distributed network with regions in upwards of 9 cortical zones (Fig. 1).

A strong possibility[34,37] is that individual differences in network anatomy may have obscured detection of these multiple PMN regions, particularly in prior analyses that relied on group

averaging. To explore this, we computed an overlap map for the 6 NSD individuals by taking the binary estimate of the PMN from the clustering analysis, and calculating how many subjects displayed a PMN region at each vertex (Fig. 1B). This analysis revealed that the prominent PCU and rPCC regions of the PMN showed overlap across all 6 individuals, whereas other regions were more variable. Notably, the aINS region also showed high overlap across most subjects, suggesting other factors may have led to this region being missed in prior analyses, such as the complex insular anatomy (e.g.,[52]).

After all statistical analyses had been performed (Fig. 3; described below), we replicated and triplicated the definition of the PMN in left-out data from the same individuals (Supp. Fig. S4). These replications again confirmed that the PMN reliably contains multiple regions beyond the core posteromedial set.

The posteromedial regions of PMN are intrinsically connected to frontal SAL regions

All subjects displayed PMN regions in the mPFC with strong connectivity to the core posteromedial components of the PMN ($r \sim 0.6$), and these were anchored at a location immediately dorsal to the apex of the genu of the corpus callosum (Fig. 1). This is interesting because this region is considered a characteristic feature of the SAL network by several accounts ([3,37,53,54]; but see[5,38]). Further, in all subjects the estimate of the PMN contained regions within the ventral aINS, another region that is characteristic of SAL.[55] This led us to consider that the two systems, SAL and PMN, may be an intrinsically connected, unified network, referred to hereafter as SAL/PMN, that has been previously studied as two systems (as suggested by[30] and see fifth Extended Data Figure in[54]).

Given this is a strong claim, to ensure generalizability, we reproduced our results in a separate cohort of extensively sampled individuals scanned at 3T using high-signal, multi-echo fMRI data. The results again supported a unified SAL/PMN (Fig. 5A). Further, we repeated network definition using a different data-driven algorithm (*k*-means clustering, maps not shown), which again preserved the distributed organization of SAL/PMN observed using MS-HBM (Fig. 1). We also examined the published analysis of UK Biobank data,[56] comprising data from 4,181 individuals, and observed that the network that included the canonical PMN regions also included all the distributed regions we report when the threshold was lowered (Fig. 4C).

Further evidence supporting the SAL/PMN as a unified network was found in subcortical connections. The posterior MTL has been considered to be part of the canonical PMN,[33,51] while the ventral striatum is identified with the canonical SAL.[55,57] Using the high- resolution 7T data, we observed that seeding from the ventral striatum revealed the full distributed SAL/PMN network (see also[31]). Similarly, seeding from the posterior MTL also revealed the full distributed SAL/PMN network (Fig. 4A & 4B). These subcortical SAL/PMN connections were also observed in UK Biobank data at lower thresholds ($z = 3$ for the posterior MTL as shown in Fig. 4C and $z = 2$ for the striatum; not shown). These analyses provide further support for SAL/PMN being a unified network. We also replicated the finding that DN-A is

connected to a more anterior part of the posterior MTL than SAL/PMN,[32,33,51] (not shown; and see[58]), further supporting a dissociation between canonical DN and PMN functions.

SAL/PMN is statistically and reproducibly dissociated from nearby networks

The observed distinction between SAL/PMN and surrounding networks was statistically tested in the left-out datasets by targeting seeds to the regions of 7 *a priori* selected networks (SAL/PMN, DN-A, DN-B, FPN-A, FPN-B, CON-A, CON-B) (Supp. Fig. S3). For all networks tested, pairwise seed-seed correlations were significantly higher within-network than between-networks when tested within each individual ($p < .05$, corrected; not shown), with few exceptions. Importantly, the SAL/PMN was statistically dissociated from the other networks (all $p < .05$, corrected) in all individuals and in both replication and triplication datasets. This result was also significant in a post-hoc group-wise analysis (Fig. 3B). The results show that the SAL/PMN is statistically dissociable from the other networks in independent data.

High-resolution data tends to preserve distributed SAL/PMN

The replication analyses of the 3T data allowed us to explore whether the resolution of the data was a factor in revealing the distributed organization of SAL/PMN. We performed clustering with higher numbers of clusters, ranging from $k = 7–50$. In all 7T NSD and some 3T DBNO participants, the cluster that included the posterior components of the SAL/PMN also included vertices within the mPFC even at the highest solution ($k = 50$; Fig. 5B, top). To further test the integrity of the SAL/PMN, we incrementally increased the number of allowable vertices in the mPFC from 1 to 50. The network's unity was preserved at the highest solution ($k = 50$) with the highest threshold (50-vertex) in 4 out of 6 participants (Fig. 5B, bottom). In DBNO subjects, the anterior and posterior components were fractionated at some level of k, suggesting that the 7T data preserved the extended SAL/PMN at higher k than the 3T data, regardless of the clustering algorithm we used. This demonstrates that as we move to higher resolution and signal-to-noise the tendency is for the distributed connections of the SAL/PMN network to be more preserved, not less. These results support that the distributed organization of SAL/PMN is veridical and more readily revealable as blurring is minimized. Importantly, both seed-based and clustering-based estimates here revealed a distributed SAL/PMN, making it unlikely to have been a result of quirks of the clustering algorithms. For both 3T and 7T datasets, the most stable solution calculated using Adjusted Rand Index in all subjects included a SAL/PMN with posterior and anterior components.

The canonical cingulo-opercular network comprises two parallel distributed networks

The separation between SAL and CON has been the subject of a nuanced debate since the networks were first identified.[53,55] In the present analyses, alongside SAL/PMN we were able to identify two networks within canonical CON regions, CON-A and CON-B (Fig. 1 & Supp. Fig. S5C). Importantly, in all subjects CON-A and CON-B contained adjacent regions in multiple cortical zones, including mPFC, IPL (Supp. Figs. S5C & S8), the insula, the RMC, and several regions of the lateral frontal cortex (a similar organization to the 'Salience/Ven Attn A' and 'Salience/Ven Attn B' networks in[38]; Fig. 1). Hence CON-A and CON-B also

appeared as parallel distributed networks in our analyses of high-resolution data, in contrast to a recent account that fractionated the canonical CON into orthogonal (e.g., anterior, lateral, central) sub-networks.[59,60] These analyses support a separation of the frontal midline into a sequence of upwards of three parallel distributed networks, with CON-B being closest to somatomotor cortices, SAL/PMN occupying more rostral mPFC, and with CON-A in between. This macroscale network sequence was also evident in the insula, with SAL/PMN being most rostral and ventral, CON-B most caudal, with CON-A in between (Supp. Figs. S5C & S8).

To ensure that these cingulo-opercular networks had been correctly identified, we investigated the relationship of this triple network sequence to a separate premotor network (PreM) that surrounds the somatomotor strip (see also[48]; Fig. 6A). In each case, the SAL/PMN, CON-A, CON-B, and PreM networks could each be separately defined using dorsomedial prefrontal seeds, with each network occupying distinct portions of the cortex throughout the brain. This confirmed the separation between all 4 networks using seeds in the anterior midline and emphasized the multi-network sequence, anchored around the central sulcus, potentially linking more somatomotor functions (PreM, CON-B) with more higher-order associative functions (CON-A, SAL/PMN).[30,48,59,60]

The SAL/PMN network *is distinct from networks within canonical default, frontoparietal control and cingulo-opercular regions in multiple cortical zones*

As has been observed in other networks,[28,46,60,61] the exact location and shape of the SAL/PMN regions varied appreciably across individuals (Fig. 1B). However, broad consistencies could also be observed in the relationship of the SAL/PMN to nearby networks. In the posteromedial cortex (Supp. Figs. S5A & S6, top panel), the SAL/PMN includes multiple regions that surround but are separable from the regions of DN-A and DN-B (see black outlines of SAL/PMN in Supp. Fig. S5A insets). In the posterior and middle cingulate cortex, SAL/PMN was consistently located posterior to FPN-A and FPN-B regions, while CON-A and CON-B regions were typically positioned within and/or across the marginal sulcus in the paracentral lobule. Similar juxtapositions were also observed in the mPFC: DN-A and DN-B were generally positioned in more rostral and ventral sites (Supp. Figs. S5A & S6), while regions of FPN-A and FPN-B were generally in more dorsal locations (Supp. Figs. S5B & S7), and regions of CON-A and CON-B were generally in more caudal locations (Supp. Figs. S5C & S8). Hence in the medial prefrontal cortex the SAL/PMN appears to sit at the confluence of DN-A, DN-B, FPN-A, FPN-B, and CON-A, with CON-B typically being separated from the SAL/PMN by CON-A. A similar juxtaposition between the networks was observed in the anterior insular (Fig. 1).

Notably, in the lateral parietal cortex, SAL/PMN regions were sometimes located exactly in between FPN-A and FPN-B, suggesting a closer correspondence between SAL/PMN and FPN-A and FPN-B than canonical DN regions.

The unified SAL/PMN preserves macroscale network sequences

We and others have previously noted that the large-scale association networks are organized into stereotyped sequences that span multiple networks.[2,3,8,28,29] The same sequence of networks can typically be observed in multiple locations, including anterior (i.e., frontal, midline, insula) and posterior (i.e., parietal, midline, temporal) cortices. The canonical (split) PMN and SAL networks break this rule. Fig. 6B shows that, when considered as a unified network, the SAL/PMN occupies the exact same position in a multi-network sequence – spanning DN-A, DN-B, SAL/PMN, FPN-A, FPN-B, CON-A and CON-B – across multiple anterior and posterior cortical zones (see arrows in Fig. 6B; and see other subjects in Fig. 1). Although the exact placement and shape of regions varies in complex ways across the brain, broadly the SAL/PMN was positioned alongside the FPNs, with the DNs on one side of the sequence and the CONs on the other. The same sequence could be observed in the anterior and posterior midline, as well as in the lateral parietal cortex, and insula (i.e., within both canonical PMN and SAL regions). A further repeat of the sequence was suggestive in the lateral temporal cortex, further supporting inclusion of the LTC into the extended SAL/PMN. This observation, of SAL/PMN regions occupying the same position along this stereotyped sequence in multiple cortical zones, is directly predicted by a unified SAL/PMN, but no such prediction arises from a split SAL and PMN.

Surface area analyses support the unified SAL/PMN

Additional support for a unified SAL/PMN was observed by comparing the surface area of each distributed network, expressed as a percentage of the total vertices in both hemispheres. Fig. 6C shows that the distributed association networks typically each occupy around 4 – 8% of the total surface area of the cerebral cortex (see also 21st figure in[46]). When SAL and PMN were considered as two separate networks, these networks were significantly smaller (all $p < .003$, corrected) than the other networks, occupying around 2% surface area. In contrast, the unified SAL/PMN network matched the expected size of the other networks ($p > .110$; n.s.). Thus, working under the assumption that the large-scale association networks occupy approximately the same size, given the resolution of the data and application of similar clustering procedures, these result are noteworthy as they suggest that dividing SAL/PMN in two may be over-splitting, particularly when considering the seed-based maps (Fig. 2)

The SAL/PMN shows a repetition enhancement effect

A unified SAL/PMN leads to the prediction that both anterior and posterior components of the network should show similar task-related responses. We tested whether the full network showed a stimulus repetition enhancement effect that is characteristic of the canonical PMN.[23,24,62]

Fig. 7A demonstrates that the map of the SAL/PMN network overlapped with regions exhibiting a repetition enhancement effect in all individuals (with the possible exception of subject S7). Notably the effect was most pronounced in posteromedial regions, but the frontal regions also showed evidence of task engagement. We conducted three targeted analyses to test whether the effect was observable in each cortical zone (see *Quantification and statistical analysis*). First, analysis of *a priori* defined seed vertices showed that in all six

individuals, the SAL/PMN exhibited a significant increase in signal for repeated images (P2 > P1 and P3 > P1; $p < .001$; P2 vs. P3, n.s.; corrected).

Second, a region-of-interest analysis focused on network regions within 5 broad cortical zones, including the posterior midline (encompassing PCU, RMC and rPCC), anterior midline (encompassing mPFC), the posterior lateral cortex (encompassing IPL), anterior lateral cortex (encompassing rPFC), and the anterior insula. The SAL/PMN had the strongest repetition enhancement effect among all networks for P2 > P1 and P3 > P1 (not P2 > P3; $p < .05$, corrected). This effect was consistent across subjects, except for S1 and S7, whose FPN-A showed a larger effect. DN-A and DN-B tended to show the opposite repetition suppression effect in both analyses, further supporting a separation between DN-A and SAL/PMN despite their close proximity in posteromedial cortex.

A third analysis used spin permutation testing to test whether the repetition enhancement effect was specific to the SAL/PMN, and was similar across frontal and posterior components of the network. Fig. 7B shows that the SAL/PMN as a whole showed a significant repetition enhancement effect (i.e., P2 > P1 and P3 > P1), and in both anterior and posterior components individually, consistently across subjects (with the exception of S7's anterior SAL/PMN regions in the P2 > P1 contrast). Averaged across subjects, the SAL/PMN also exhibited the largest repetition enhancement effect of all the networks (Fig. 7C). Other networks did not show significant effects, with the exception of FPN-A, which showed a similar but weaker pattern to SAL/PMN, and the anterior portion of DN-B which also showed a small significant increase.

Discussion

We studied the detailed anatomy of large-scale networks using high-field and high-resolution 7T fMRI. We found that, when defined within an individual, the canonical PMN is a distributed network that contains regions in upwards of 9 cortical zones (Fig. 1), including regions previously considered part of the canonical SAL network, indicating that the two networks form a unified 'SAL/PMN' network.[30] We show that the SAL/PMN is closely interdigitated with, but clearly and statistically dissociable from, other nearby large-scale networks (Fig. 3 and Supp. Figs. S5–S8). We further show that the entire SAL/PMN network, including anterior and posterior components, can be defined from subcortical seeds targeting the posterior MTL and ventral striatum (Fig. 4AB; see[31]), and shows evidence of task engagement in a recognition task typically associated with the PMN (Fig. 7; but see[13]). The findings were confirmed in all 6 7T NSD subjects analyzed (Fig. 1), were consistent across analysis procedures (Figs. 1–2, 4AB), were replicated and triplicated in the same individuals (Fig. 3 and Supp. Fig. S4), and were further replicated in 2 independent datasets (Figs. 4C and 5A). The results confirm that SAL/PMN, when considered as a unified network, shows a distributed architecture which better matches the parallel network organization characteristic of association cortex.[2] Our results suggest that, like the other association networks, the SAL/PMN may have emerged through a process of fractionation of a prototypical distributed network architecture during development.[29,63]

The SAL/PMN as a parallel distributed network

In all individuals, our exploration revealed a distributed network including regions in upwards of 9 cortical zones, including PCU, rPCC, RMC, mPFC, vmPFC, rPFC, dPFC, aINS, and IPL (see dashed and dotted boxes in Fig. 1B). The resulting organization encompassed canonical PMN and SAL regions, suggested that the two networks are actually a unified system when imaged at sufficiently high resolution and signal to noise. Sometimes the network regions were small (e.g., see IPL and vmPFC in Fig. 1), and would have been overlooked if their clearer presence in other subjects were not suggestive. Notably, the regions with the most overlap were also those that have most often been ascribed to the canonical PMN: the PCU and rPCC (Fig. 1B).[23,34,37] Other regions, such as the IPL and rPFC, showed more variability across individuals. Similarly, although the rPFC and mPFC regions were relatively large, they were more dispersed, leading to less overlap across individuals. This provides a compelling explanation for why group-averaged data may have split the SAL/PMN into two networks: canonical PMN regions in the posteromedial cortices show high consistency across individuals, while frontal regions are much more variable. This could lead to a division of frontal and posterior components when group-wise analyses are conducted, due to blurring across misaligned functional regions in anterior components of SAL/PMN. These findings underscore the need for individual-level network estimation.

However, recent within-subject network analyses have also sometimes considered the anterior and posterior parts of the SAL/PMN as separate networks.[37] Our results showed that the lower resolution 3T data tended to split SAL/PMN into two networks more often and at a lower number of clusters than the higher resolution 7T data, regardless of algorithm used (Fig. 5B). This supports that the ability to define smaller network regions in the high-resolution 7T data may be key in characterizing the distributed connections between the anterior and posterior components of SAL/PMN. This may be because the anterior regions are smaller than the prominent posteromedial regions and/or potentially more prone to partial volume effects. Therefore, even within individuals blurring may have led to the SAL/PMN being over-split in past work.

An interesting observation was that some individuals showed limited evidence of a SAL/PMN region in the lateral temporal cortex (LTC). This would be unremarkable given the small size of the region identified, its low correlation values, and its inconsistency across individuals. However, this putative region was located right next to a zone of signal dropout (Supp. Fig. S1), raising the possibility that a lateral temporal SAL/PMN region may exist that has been missed. Supporting this, the LTC region was also evident in a large group-average analysis of n = 4,181 individuals in the UK Biobank at a lower threshold (z=3; Fig. 4C), and the task-activation map during the recognition task (Fig. 7A). There are also reasons to think that this part of the brain should contain a SAL/PMN region. Our analyses suggest that the SAL/PMN is closely linked to FPN-A and FPN-B (Supp. Figs. S5B & S7), both of which contain lateral temporal regions approximately where this putative SAL/PMN region might be (Figs. 1 & 5A; and see [1,3,5,28]; see also Fig. 6B). Analysis of multi-echo data, which theoretically improves signal at dropout regions, provided similar, suggestive support for the presence of this LTC region in 7 out of 8 subjects (Supp. Fig. S9). These observations

underscore that technological advances in neuroimaging, such as the advent of higher-resolution, individualized, and lower dropout approaches, can provide valuable refinements to prior knowledge.[3,5]

Variability across individuals

While we focused on functional anatomic features that were consistent across individuals and methods, certain regions exhibited more heterogeneity than others (Fig. 1B). For instance, although all subjects displayed regions of the SAL/PMN in each of the broad "zones" indicated in Fig. 1B, some regions such as the rPFC exhibited more variation across subjects. Prior work has suggested that association cortex is more variable across individuals in functional organization than unimodal cortex,[64] and that individuals can vary considerably in the size, shape, location, and topography of functional regions.[39,65] One proposal is that such heterogeneity may result from activity-dependent processes during development.[29,63] DiNicola & Buckner[29] describe a process by which an archetypal distributed network motif is fractionated into functional regions as the cortex expands. This fractionation into regions may be somewhat stochastic at a fine scale, making it unclear how physiologically relevant such fine-scale differences are. However, recent studies support that some features of individual differences are significant for cognition and mental health.[38,54]

Relationship to other networks

Detailed analysis suggests that the SAL/PMN sits at the confluence of multiple networks, including DN-A, DN-B, FPN-A, FPN-B, CON-A, and CON-B. The SAL/PMN occupies regions that are often completely distinct from other nearby networks, despite the complex fine-scale anatomy on display (Supp. Figs. S5–S8). Importantly, this organization was observed using both data-driven clustering and seed-based analyses of functional connectivity, the latter of which does not enforce a winner-takes-all assignment. Despite the complex and detailed anatomy of juxtaposed regions, seeds targeted to each network in 5 cortical zones using the discovery dataset statistically dissociated the networks in independent data, both at the group and individual level, and in both the replication and triplication datasets (Fig. 3). These results indicate that the SAL/PMN is as distinct from other large-scale networks as the other networks are distinct from each other.

Prior estimates have diverged in considering the canonical PMN as a sub-system of the canonical default (e.g.,[3]) or frontoparietal control networks (e.g.,[5]). On the other hand, there has been ongoing confusion regarding the relationship between the SAL and CON networks.[55,66] Here, in the posteromedial cortex (Supp. Figs. 5A & S6), three regions of the SAL/PMN – at or near the PCU, rPCC, and RMC – were found to encircle the regions of DN-A and DN-B. The prominence of the PCU and rPCC regions may have led to a stronger association in the literature between the SAL/PMN and the default network. However, the same rPCC region of the SAL/PMN is also juxtaposed with regions of FPN-A and FPN-B as one moves rostrally along the callosal sulcus (Fig. 1). Our data shows that the SAL/PMN is closely juxtaposed next to frontoparietal control network regions in the posteromedial (Fig. 1), inferior parietal, and medial prefrontal cortices (Supp. Figs. 5B & S7). In the IPL, the

SAL/PMN more often was juxtaposed with FPN-A and FPN-B, remarkably filling the small gap between the FPN-A and FPN-B in many individuals, and often not bordering DN-A or DN-B. This variability, where the SAL/PMN borders DN-A and DN-B in some regions but not others, may be a result of higher variation in functional organization found in association cortex,[39,67,68] or could be suggestive of further sub-structure within what we are defining as the SAL/PMN. Alternatively, these findings could suggest that the SAL/PMN is more closely linked to frontoparietal control functions. Supporting this, the functional connectivity of SAL/PMN was anti-correlated (i.e., showing negative correlations) with DN-A and DN-B (Fig. 3), but not FPN-A and FPN-B.

In line with previous studies, analysis of a continuous recognition task provided further evidence for the unified SAL/PMN and for the separation between SAL/PMN and canonical default network regions. We observed the repetition enhancement effect within the SAL/PMN, both in anterior and posterior components (Fig. 7), but observed a trend in the opposite direction for DN-A.[69] In addition, we also observed a significant, if weaker, repetition enhancement effect in FPN-A (Fig. 7C). These results, along with the close juxtaposition between SAL/PMN and frontoparietal control networks in regions, again suggest that the SAL/PMN may be more closely aligned functionally to the frontoparietal control than default network systems. Thus, the SAL/PMN and FPN systems may serve overlapping functional domains to some degree, which could be reflected in the spatial overlap between these networks,[70] with the SAL/PMN potentially representing domain-general processes that are related to salience processing and novelty detection. Notably, the task effects were less robust in some areas, such as aINS and dorsal mPFC, and adjacent regions that were likely in FPN-A showed clearer evidence of task activation, raising the concern that SAL/PMN activation effects here could be a result of signal bleeding from adjacent areas. However, given that other networks adjacent to FPN-A, such as FPN-B and CON-A, did not show task effects (Fig. 7C), and that SAL/PMN regions farther from FPN-A (e.g., in rostral mPFC) did exhibit task effects, this concern is minimized.

A final set of analyses provided evidence that, when considering broad multi-network sequences that are observable in multiple cortical zones (Fig. 6B), the anterior and posterior components of SAL/PMN were located in precisely the same position along the sequence. This observation is uniquely predicted by considering that the anterior and posterior components form part of a larger ‘parent’ SAL/PMN network. In contrast, a split SAL and PMN would not lead to this prediction. Hence, our observations help reconcile two discrepancies on that the SAL and PMN networks have differed in unusual ways from the properties observed of other association networks.

Although our data suggests that the PMN and SAL form a unified network, it remains a possibility that there could be substructure within the network. For instance, although our recognition task analysis showed that anterior and posterior regions exhibited similar responses, the effects were stronger in posteromedial region, which could represent true differences in their relative functions. Our results support that the unified SAL/PMN fits particularly well with the expected organization of other association networks, but it remains

possible that there is sub-specialization within the network. For instance, one way in which networks may specialize is in fractionating a larger 'parent' network into anterior and posterior components. In other words, one might interpret these results as suggesting that SAL and PMN may share a 'privileged connection' rather than forming a single network. That said, the differences in the magnitude of task response observed in SAL and PMN do not diminish our findings that these networks are strongly correlated in the task-free resting-state analyses. Future studies should seek to ascertain whether there is indeed evidence for functional specialization between anterior and posterior components of SAL/PMN using methods that can capture the fine-scale distinctions we describe here at high resolution.

Limitations of the Study

Although care was taken to ensure that the networks were accurately identified and were consistent across individuals and estimation methods, it is possible that in some cases our clustering analyses over-split certain networks. For instance, in the case of three individuals (S1, S6 & S7), the clustering solution (i.e., value of *k*) that allowed us to separate the SAL/PMN also led to a division of the canonical default network into three networks, rather than two as per our previous investigations.[28] In these individuals, we took the two networks that were closest to the PMN and labelled them "DN-A" and "DN-B"; however, the results should be interpreted accordingly: these subjects were missing some core components of DN-A, such as the key region extending into ventral posterior cingulate and retrosplenial cortex (see Fig. 1 right column;[28,47]). Hence in these participants "DN-A" should be considered with this caveat. Note this does not affect the claims about the SAL/PMN being distinct and distributed, and that this over-splitting was not present in the other three subjects. The analyses here also focus heavily on resting-state functional connectivity, and need to be supported by further task-based analyses within extensively sampled individuals, at high-resolution, to test whether high-resolution analyses support further substructure within the SAL/PMN including division into anterior and posterior components. Similarly, the recognition task used here did not dissociate SAL/PMN from FPN-A (Fig. 7), whereas more targeted tasks may be able to.

Conclusion

Here we provide evidence that the SAL/PMN is a unified, distributed network with regions in upwards of 9 cortical zones. We show that the SAL/PMN is closely juxtaposed with approximately 6 large-scale networks (DN-A, DN-B, FPN-A, FPN-B, CON-A, CON-B), but provide evidence for a closer link between the SAL/PMN and frontoparietal control regions than default network regions based on spatial proximity and similarity of task-evoked responses. The results address a discrepancy in our understanding of the large-scale networks, particularly the canonical PMN and SAL which have historically not shared the distributed organization characteristic of association cortex; an observation that is reconciled by a unified SAL/PMN. The findings underscore the need for individualized, high-resolution, and high-field fMRI studies that provide greater separation between the tightly interwoven networks that populate the cortical mantle.

Resource Availability

Lead Contact

Further information and requests for resources should be directed to and will be fulfilled by the lead contact, Young Hye Kwon (younghye.kwon@northwestern.edu).

Materials Availability

This study did not generate new materials.

Data and Code Availability

All data needed to evaluate the conclusions in the paper are present in the paper and/or the Supplementary Materials. All source data from the NSD Dataset, are publicly available at http://naturalscenesdataset.org. The ICA-derived group-level functional maps from UK Biobank are available at https://www.fmrib.ox.ac.uk/ukbiobank/group_means/rfMRI_ICA_d25_good_nodes.html. All custom code has been deposited at GitHub and is publicly available at [10.5281/zenodo.14278880] as of the date of publication. Accession numbers are listed in the key resources table. The independent dataset used for replication is available from the lead contact upon request.

Acknowledgments

We thank Dr. Randy Buckner for helpful discussions regarding the framing of the results. This work was supported in part by National Institute of Mental Health grant R00 MH117226 (to R.M.B); an Alzheimer's Disease Core Center grant (P30 AG013854; R.M.B.) from the National Institute on Aging to Northwestern University, Chicago, Illinois.; a training award T32 NS047987 (to J.J.S and N.A); the William Orr Dingwall Foundations of Language Fellowship (to J.J.S); National Institutes of Health R01 MH118370 and National Science Foundation (NSF) award NSFCAREER 2305698 (to. C.G); National Institutes of Health grant (NIH) R01EY034118 (K.K.). Collection of the NSD dataset was supported by NSF IIS-1822683 (K.K.) and NSF IIS-1822929. B.T.T.Y. is supported by the NUS Yong Loo Lin School of Medicine (NUHSRO/2020/124/TMR/LOA), the Singapore National Medical Research Council (NMRC) LCG (OFLCG19May-0035), NMRC CTG-IIT (CTGIIT23jan-0001), NMRC OF-IRG (OFIRG24jan-0030), NMRC STaR (STaR20nov-0003), Singapore Ministry of Health (MOH) Centre Grant (CG21APR1009), the Temasek Foundation (TF2223-IMH-01), and the United States National Institutes of Health (R01MH133334). K.Y. is supported by the National Research Foundation of Korea (NRF) grant funded by the Korea government (MSIT) (RS-2024-00335670) and by a grant of the Korea Dementia Research Project through the Korea Dementia Research Center (KDRC), funded by the Ministry of Health & Welfare and Ministry of Science and ICT, Republic of Korea (RS-2024-00339665). The content is solely the responsibility of the authors and does not represent the official views of the National Institutes of Health, National Science Foundation, Singapore NMRC, Singapore MOH, Temasek Foundation, Korea NRF or any funders. This research was supported in part through the computational resources and staff contributions provided by the Center for Translational Imaging and Quest high performance computing facility at Northwestern University which is jointly supported by the Office of the Provost, the Office for Research, and Northwestern University Information Technology.

Author contributions

Conceptualization: YK, RMB

Methodology: YK, RMB
Data curation and investigation: KK, JJS, NA, DE, AMH, ML, RMB
Formal analysis: YK, NA, KK, RMB
Visualization: YK, RMB
Writing–original draft: YK, RMB
Writing–review & editing: YK, JJS, AMH, KY, BTTY, KK, CG, RMB
Supervision: RMB

Declaration of interests

Authors declare no competing interests.

Main figure titles and legends

Fig. 1: High-resolution functional connectivity within individuals reveals that the posteromedial regions of the PMN form a distributed network that includes regions typically ascribed to the SAL, suggesting that PMN and SAL form a unified "SAL/PMN" network. **A.** The left column shows the network estimated using a seed-based approach in each individual (rows) using seeds (white circles) selected from the rostral prefrontal cortex (rPFC). The right column shows the same distribution of SAL/PMN regions (dark blue network) was observed using a data-driven clustering approach. Clustering was used to define 7 *a priori* selected networks in the vicinity of the SAL/PMN, including DN-A, DN-B, FPN-A, FPN-B, CON-A, and CON-B. **B.** An overlap map of SAL/PMN from each individual's clustering analysis. Dashed and dotted boxes refer to key cortical zones where each subject displayed a region of SAL/PMN across methods. Dotted boxes indicate canonical SAL regions. dPFC; dorsal prefrontal cortex, aINS; anterior insula, IPL; inferior parietal lobule, RMC; ramus marginalis of the cingulate sulcus, vmPFC; ventromedial prefrontal cortex. *k;* number of clusters used to define networks in each participant, though note the solution was stable across multiple levels of clustering.

Fig. 2: Seed-based functional connectivity at high resolution reproducibly defines SAL/PMN from multiple cortical zones. Five estimates of the SAL/PMN, seeded from five cortical zones, are shown in two representative participants (S2 and S3; the remaining 4 participant are shown in Supp. Fig. S2) confirmed the distributed organization of the SAL/PMN. Seeds are shown in white circles.

Fig. 3: The SAL/PMN is statistically dissociated from nearby networks in left out datasets. **A.** The larger matrix on the left shows the cross-correlation matrix averaged across all subjects, and the smaller matrices to the right show the correlations in each subject (excluding S2 who only provided a discovery dataset). The upper triangle of each matrix represents correlations in the replication dataset, and the lower triangle represents the triplication dataset for individuals who provided sufficient data. **B.** The plots show the group-averaged comparisons between within- and across-network seed-seed correlations in the replication (top) and triplication (bottom) datasets. Each dot represents a different individual, showing the average correlation for all seeds within each network, and across all runs (paired t-tests, * $p < .05$, corrected). The SAL/PMN showed strong within-network correlations, to the same level as other networks.

Fig. 4: The unified SAL/PMN was confirmed through analysis of subcortical connectivity and the UK Biobank data. A. SAL/PMN defined from seeds in the posterior MTL (considered part of the canonical PMN) shows clear connectivity within the anterior

components of the network (considered part of the canonical SAL). **B.** Seeds targeting the ventral striatum (see black arrows) and mPFC (considered part of the canonical SAL) shows clear connectivity with posteromedial regions (considered part of the canonical PMN). White circles indicate the seed location, and dotted white circles indicate an approximate location of seeds defined in the volume. Three representative subjects are shown (S2, S3, and S4). **C.** Group-averaged resting-state functional connectivity maps from UK Biobank[56] recapitulate the distributed SAL/PMN when examined at lower thresholds (z = 3; see white labels) than the default setting (z = 5). Sagittal views show "component 21" from an independent component analysis at 25-dimensions.

Fig. 5: The unified SAL/PMN network is replicated in an independent 3T multi-echo dataset, and indicates that higher resolution 7T data more readily reveals the full distributed network. A. Functional connectivity procedures were replicated in the independent 3T DBNO dataset, and each subject showed the full distributed SAL/PMN network. **B.** (Top) The plot shows *k* values at which the SAL/PMN split into anterior and posterior components in the 3T and 7T datasets, using MS-HBM and *k*-means clustering algorithms. Each data point represents an individual subject. The network that contained the posteromedial PMN regions was considered unified if one or more vertices were present within the mPFC region of the canonical SAL. (Bottom) Increasing the number of mPFC vertices that count as preserving the distributed network shows that even using more stringent criteria the high-resolution data more readily preserved the distributed network.

Fig. 6: A unified SAL/PMN conserves a multi-network sequence in multiple cortical territories, and better matches the other distributed networks in surface area. A. Seeds were chosen from the dorsomedial prefrontal cortex in an anterior-posterior progression to target SAL/PMN, CON-A, CON-B, and the premotor network (PreM) in two individuals (S2 and S7). White lines serve as hand-drawn landmarks for comparing across panels, to show how each network occupies distinct portions of the cortex despite being defined from nearby seeds. White circles indicate the seed used to define the network shown in that panel, and black hollow circles represent seeds for the other networks shown. **B.** Clustering-derived network maps from an example subject (S2) show that macroscale network sequences are conserved in multiple cortical territories when the SAL/PMN is considered unified. **C.** Bar graphs show the surface area when SAL/PMN is considered as a unified network (left) and when the network is split into anterior (ant.; canonical SAL) and posterior (pos.; canonical PMN) regions (one-way ANOVA, **p < .01, ***p < .001, corrected, n.s.; not significant).

Fig. 7: The unified SAL/PMN shows a repetition enhancement effect throughout the distributed network. A. Maps display z-scored *t*-values representing the contrast of P2 > P1. The boundaries of the SAL/PMN (from Fig. 1) are shown in black. **B.** A spin test was performed using the averaged task-related beta values calculated for SAL/PMN as a whole ("Unified") and split into anteromedial ("Ant.") and posteromedial ("Pos.") components. The anteromedial and posteromedial regions were divided according to the dotted line shown in the box. Permuted *t*-values are shown for P2 > P1 (pink), P3 > P1 (green), and P3 > P2 (grey), with the observed *t* -value for each contrast condition is shown as a red diamond (1,000 iterations, alpha = 0.05; n.s.; not significant). **C.** The bar graph shows the mean *t*-values for each region within each network, averaged across all subjects and contrasts (error bars represent +/- SEM). Each of the SAL/PMN regions showed an increase (i.e., the repetition enhancement effect), as did FPN-A (one-sample t-test, *p < .05, **p < .01).

STAR★Methods

Key resources table

The key resources table (KRT) serves to highlight materials and resources essential to reproduce results presented in the manuscript. The items in the table must also be reported alongside the description of their use in the method details section. Literature cited within the KRT must be included in the references list. Please do not add custom headings or subheadings to the KRT. We highly recommend using RRIDs (see https://scicrunch.org/resources) as the identifier for antibodies and model organisms in the KRT. To create the KRT, please use the template below or the KRT webform. See the more detailed Word table template document for examples of how to list items.

REAGENT or RESOURCE	SOURCE	IDENTIFIER
Antibodies		
Bacterial and virus strains		
Biological samples		
Chemicals, peptides, and recombinant proteins		
Critical commercial assays		
Deposited data		
Natural Scenes Dataset	Allen et al.[64]	http://naturalscenesdataset.org
Detailed Brain Network Organization dataset	This paper	Upon request
UK Biobank	Miller et al.[65]	https://www.fmrib.ox.ac.uk/ukbiobank/group_means/rfMRI_ICA_d25_good_nodes.html

Custom codes	This paper	10.5281/zenodo.14278880
Experimental models: Cell lines		
Experimental models: Organisms/strains		
Oligonucleotides		
Recombinant DNA		
Software and algorithms		
MATLAB	MathWorks	https://www.mathworks.com/products/matlab.html
FreeSurfer	Fischl [87]	https://surfer.nmr.mgh.harvard.edu/
Connectome Workbench	Marcus et al.[88]	https://www.humanconnectome.org/
PALM	Winkler et al.[95]	https://www.nitrc.org/projects/palm/
Other		

Experimental model and study participant details

Participants

For participants from the Natural Scenes Dataset (NSD[71]) six participants out of eight were included in this study. Two participants (S5 and S8) were excluded due to excessive head

motion during resting state runs, resulting in a final sample of six participants (S1-S4, S6, and S7; 4 females, age range 23-30 years, mean age = 26.8 ± 2.8 years). Each participant provided approximately 30-40 fMRI sessions, with an average of 2.0 hours of resting-state (passive fixation) and 38.5 hours of active task fMRI data per participant. MRI sessions were collected approximately once per week. More details about participant information can be found in[71].

For the DBNO data, ten participants were recruited for an MRI study at Northwestern Memorial Hospital. Following an initial trial period, intended to allow participants to become familiar with the scanning procedures before committing to the full study, and for the study team to vet participants who did not comply with instructions, two participants were excluded for excessive head motion. The eight participants who were included in this study were native English speakers, neurologically healthy, and had normal or corrected-to-normal vision (4 females, age range 22–36 years, mean age = 26.8 ± 5.3 years). Participants provided written informed consent in compliance with procedures approved by the Northwestern University Institutional Review Board and were paid for their participation. The experiment consisted of eight sessions. During each session, participants completed two 7-min resting-state (passive fixation) runs which were collected as the first and final runs in each session. This resulted in a total of 112 minutes (2 runs x 8 sessions x 7 min) of resting-state data per participant. Participants completed a subset of a total of 9 active tasks between the two resting-state runs in each session, but we analyzed only the resting-state data in the present study.

Method details

Main analysis of 7T fMRI data from the NSD

Overview

Data from each participant were divided into a discovery dataset, for exploratory analysis, and replication and triplication datasets for validation (see Supplementary Table S1). The SAL/PMN was initially defined in the discovery dataset from each participant using a manually selected seed-based approach, followed by data-driven clustering. We also defined 6 other *a priori* selected networks, DN-A, DN-B, FPN-A, FPN-B, CON-A, and CON-B, chosen based on their theoretical relevance and spatial proximity to the SAL/PMN along the cortex. We then statistically tested the separation of the SAL/PMN from these adjacent networks in the left-out, validation datasets. Following statistical testing, we replicated and triplicated the definition of the SAL/PMN in the left-out datasets. Finally, to confirm the functional properties of the SAL/PMN we assessed the networks for the 'repetition enhancement' effect by comparing activity elicited by viewing repeated images in the NSD dataset.

Resting-state fMRI

Two resting-state fMRI runs were collected per session, one before and one after the main NSD tasks (further details in[71]). Each resting-state run lasted 5 minutes, and a total of 100-180 minutes of resting-state data were acquired over 10-18 sessions for each participant. During the first resting-state run of each session, participants were told to remain awake and

fixate their gaze on a centrally presented white crosshair. In the second resting-state run, participants were presented with a red crosshair at the beginning and instructed to take a deep breath when the crosshair turned red. After this cued breathing period, which occurred only once, participants were instructed to fixate for the remainder of the run. Both types of runs were treated as resting-state data here and counterbalanced first and second runs were allocated to each dataset (discovery, replication, triplication).

MRI data acquisition, processing and quality control

Functional images were collected using a 7T Siemens Magnetom MR scanner at the Center for Magnetic Resonance Research at the University of Minnesota. Blood-oxygenation-level-dependent (BOLD) images were collected using gradient-echo echo-planar imaging (EPI) at 1.8-mm isotropic resolution with whole-brain coverage with the following parameters: TR = 1,600 ms, TE = 22.0 ms, Flip angle 62 degrees, FOV = 216 mm (FE) × 216 mm (PE), slice thickness 1.8 mm, slice gap 0 mm, matrix size 120 × 120, echo spacing 0.66 ms, bandwidth 1,736 Hz per pixel, partial Fourier 7/8, iPAT 2, multiband slice acceleration factor = 3, and 84 slices acquired in the axial plane. Dual-echo fieldmaps were collected for post hoc correction of EPI spatial distortion. Pre-processed versions of the data are shared in the NSD (http://naturalscenesdataset.org), which include steps to correct for slice acquisition timing, alignment of data from each TR to correct for head motion within a run, alignment across sessions, correction for EPI distortion, all performed within one interpolation step. Detailed information on preprocessing procedures can be found in[71].

We performed quality control on the NSD resting-state data and excluded runs that did not pass rigorous criteria for head motion. Whole runs were automatically excluded if maximum framewise displacement (FD) was greater than 0.4 mm, or maximum absolute motion was greater than 2.0 mm. We also visually inspected any runs with maximum FD > 0.2 mm or a maximum absolute motion > 1 mm, and excluded any that exhibited visible movement. This resulted in a total of between 6-35 resting-state runs per participant (S1: 35 runs; S2: 6; S3: 16; S4: 12; S6: 19; and S7: 18). For the five participants with 12 or more included runs, the data were divided into two or three groups: a discovery dataset plus replication and triplication datasets (see Supplementary Table S1).

For functional connectivity analysis, we performed additional preprocessing on the resting-state data following procedures outlined in[47]. Nuisance variables were regressed out, including six parameters to account for head motion, as well as whole-brain, ventricular, and deep white matter signal, and temporal derivatives. Nuisance regression was performed using 3dTproject (AFNI version 2016.09.04.1341;[72]) on native-space-projected BOLD data resampled to 1mm isotropic resolution (i.e., the 'func1pt0mm' version of the NSD data). Data were bandpass filtered at 0.01–0.1Hz (using 3dBandpass from AFNI). Next, we projected the data onto a standardized cortical surface containing 163,842 vertices (fsaverage7) per hemisphere using FreeSurfer's vol2surf command[73] and smoothed along the surface using a 2.5mm FWHM kernel. The highest resolution cortical mesh was used to minimize blurring and preserve fine-scale distinctions between networks. The smoothing kernel was chosen by eye based on preliminary analyses on one individual, carefully

assessing the trade-off between minimizing smoothing (i.e., preserving details), maximizing correlation values, and minimizing noise or 'speckling' in randomly chosen seed-based correlation maps in the exploratory data. Functional connectivity matrices were estimated in each participant by computing vertex-vertex Pearson's product-moment correlation for each run, z normalizing, averaging across runs within each dataset in each individual, then converting back to r values. These matrices were then used for network estimation[28] for manual seed-selection using the Connectome Workbench[74] and for data-driven clustering.

Seed-based functional connectivity analysis

Our initial analyses sought to identify the PMN within each individual, anchoring on the spatial distribution of key component regions previously reported.[23,39] The two key components were the prominent PCU and rPCC regions that most consistently comprise the PMN.[34] We initially hand-selected seeds in the lateral PFC (a seed in our analyses refers to a single vertex in the mesh representing the cortical surface). This was done (i) to allow comparison to our previous seed-based analyses targeting other association networks within individuals,[17,28,46] where networks were distinguished using nearby seeds within lateral PFC to bias the correlation patterns to be similar to each other and ensure we were truly observing dissociable networks, (ii) to allow long-distance correlation patterns to be appreciated (e.g., at our key component regions) without the confound of local blurring near the seed, and (iii) following initial observations that the PMN could be reliably defined from seeds in the PFC. We searched for a seed that recapitulated the organization of the PMN by targeting seeds to five cortical zones in each individual. The seed locations were selected based on the network regions revealed by the rPFC seed, hence this analysis provided confirmation that the rPFC seed was not unique in revealing a distributed network, but rather the entire network could be defined from multiple cortical locations, emphasizing its distributed structure. The zones include the rPFC, aINS, IPL, posteromedial cortex (posterior cingulate, precuneus, cuneus and retrosplenial cortices), and mPFC. The zones were chosen to target both anterior and posterior components of the network where PMN regions were large enough to be seeded. These seeds replicated the detailed organization of the PMN (correlation maps thresholded at $r > 0.2$), including confirmation of a PMN region in the rPFC (Fig. 2 and Supp. Fig. S2). We also targeted six other networks, DN-A, DN-B, FPN-A, FPN-B, CON-A, and CON-B, with seeds selected in the same 5 cortical zones (with the exception of DN-A, for which no region could be found in the aINS zone; Supp. Figs. S5A & S6). These seeds were used to statistically test for a dissociation in the correlation between the networks in each individual using the left-out replication and triplication datasets.

The separation between SAL and CON has been a topic of a nuanced and ongoing discussion since their initial identification. To ensure the accurate identification of cingulo-opercular networks, we examined the relationship of the network sequence (i.e., SAL, CON-A, and CON-B) and a separate premotor network (PreM) that surrounds the somatomotor strip (see exploration of this region in[48]; Fig. 6A). Seeds were manually selected from the dorsomedial prefrontal cortex in the two individuals that seemed to provide particularly good separation between networks during seed-based analyses (S2, S7; based on observer impressions by authors Y.H.K. and D.E).

Clustering approach

A multi-session hierarchical Bayesian model (MS-HBM) parcellation method[75] was employed for confirmation of network organization. This approach provides individual-specific network estimates by integrating priors from multiple levels (e.g., group atlas, cross-individual and cross-run variation) to stabilize network estimates. The MS-HBM parcellation method was applied to define networks using the discovery dataset. In each individual, we used a *k* value (i.e., number of clusters) between 7–50 and selected the lowest solution that best matched the networks observed in the seed-based analysis, respecting that the same value of *k* can over-split or over-lump networks in different individuals. Namely, the lowest value of *k* that separated the SAL/PMN from other networks – with an initial focus on SAL/PMN's separation from FPN-A and FPN-B – as observed in the seed-based approach was taken as the solution. Notably, to achieve separation of the SAL/PMN and match our seed-based observations, in some subjects a level of *k* was used that over-split our expected breakdown of DN-A (i.e., note diminished DN-A region in the retrosplenial cortex in subjects S1, S6 & S7 in Supp. Fig. S6). The highlighted details in Supp. Fig. S6 allow appreciation of the differences between seed-based and clustering solutions of DN-A in these subjects. Note that in all subjects the clustering estimate of the SAL/PMN overlapped closely with seed-based estimates (see multiple details in Supp. Figs. S5–S8), indicating that this over-splitting of DN-A did not affect the estimate of the SAL/PMN. The clustering analysis provided a data-driven confirmation of the patterns observed in the manual seed-based approach, while minimizing observer bias. The two approaches provided converging solutions and confirmed the PMN as a distributed network that is distinct from surrounding networks.

Volume-based functional connectivity analysis

To examine subcortical regions of SAL/PMN in the volume, we estimated the networks using a seed-based approach. We analyzed native-space projected volumetric BOLD data from the NSD that was preprocessed for functional connectivity analysis. Based on initial assessments of data quality and the strength of correlation maps (outlined in[58]), a 2.5-mm FWHM smoothing kernel was applied to five individuals (S1-S4, S6) and a 2-mm FWHM smoothing kernel was applied to one individual (S7) using fslmaths (FSL v6.0.3).[76] Data were analyzed and visualized using AFNI's InstaCorr.[72,77] Pearson's product-moment correlation coefficient was computed between all voxel pairs within a whole-brain brain mask for each run of resting-state data using 3dSetUpGroupInCorr. The correlation matrices were then Fisher transformed prior to cross-run averaging with 3dGroupInCorr to create a single, cross-run average functional connectivity matrix for each dataset from each individual. We manually selected individual voxels as seeds in the MTL, mPFC, PMC, and striatum, and observed their associated whole-brain correlation maps using AFNI. This process was used to define SAL/PMN in the discovery dataset. Volume-defined seed-based correlation maps were then projected to the cortical surface for comparison to the surface-defined network maps in the main analyses (e.g., Fig. 1)

Continuous recognition task

We sought to confirm that the SAL/PMN identified here displayed functional properties characteristically ascribed to the PMN (e.g.,[23]). Namely, the PMN shows a repetition enhancement effect, where the perceived familiarity of a stimulus (e.g., an image) is associated with increased responses. This response includes a 'flip' from below-baseline activity during initial presentation of novel images, to above-baseline increased activity for repeated presentations. To confirm the functional characteristics of the PMN, task data from the NSD experiment, a continuous recognition task, were analyzed. Participants viewed a series of color natural scene images and were asked to respond every time they saw an image while undergoing scanning. Participants were instructed to press a button with their right index finger if they thought the presented image was new or press another button with their right middle finger if the presented image had been shown previously. Each run included 62-63 trials, with an image presented every 3 seconds, followed by 1s fixation period. Twelve runs were collected in each session, yielding a total of 750 trials per session. Each participant underwent 30-40 sessions over one year (S1: 40 sessions; S2: 40; S3: 32; S4: 30; S6: 32; and S7: 40; though the last 3 sessions from each participant had not yet been released and were not analyzed here). More details on the task design are provided in[71]. The large number of trials available (ranging from 22,500 to 30,000 trials per participant) allows reliable exploration of repetition effects. The experiment consisted of 10,000 distinct images, each of which was presented up to three times throughout the experiment, depending on the number of completed sessions by a participant. Participants also completed a variety of behavioral measures, a final memory test, and an image-similarity assessment after the scan, not analyzed in the present study.

The NSD public release includes beta maps for each trial of the continuous recognition task (representing the percent BOLD signal change evoked by each trial relative to a baseline), as well as mean FD and voxel-wise tSNR for quality control purposes. We excluded runs with mean FD greater than 0.16 mm and tSNR lower than 20. We compared betas (beta version 3 provided in the NSD) from trials containing repeated versus novel presentations of the same images, restricting the analysis to correct responses only. To focus on short-term recognition memory, and avoid the increased variance of comparing data across sessions, we considered only images that were presented 3 times within the same session. The within-session repeats were also more likely to be recognized as familiar (within-session hit rate = .98, across-session hit rate = .72, $p < .001$). By design, participants were presented with the 'new' condition more frequently than the 'old' condition during the initial sessions, and were presented with the 'old' condition more often during the later sessions. To avoid odd-ball effects, we only included sessions where the difference between the 'new' and 'old' conditions had a ratio less than 0.3. In other words, only sessions in which both trial types were relatively balanced, with neither trial type comprising less than 35% or more than 65% of the total trials, were included in the analysis. As a result, 14 sessions were included in the analysis for each individual. Similar results were obtained in an initial analysis that included all sessions.

Trials were divided into three types relating to first (P1), second (P2), and third (P3) presentation of each image. Only trials with correct responses were included in the analysis; specifically, trials where images were correctly identified as novel in their first appearance (i.e.,

correct rejections) and correctly identified as repeats in the second and third appearances (i.e., hits; see Quantification and Statistical Analysis).

Validation in an independent dataset at 3T

Overview

We reproduced the definition of the PMN in an independent 3T MRI dataset containing 8 extensively sampled participants collected at Northwestern University as part of the Detailed Brain Network Organization (DBNO) study. Data were quality controlled and runs that did not pass the same criteria as the NSD data for head motion were excluded. This led to a total of between 10-16 resting-state runs per participant (S1: 16 runs; S2: 16; S3: 16; S4: 16; S5: 10; S6: 15; S7: 14; and S8: 14). For the seven participants with more than 12 good quality runs, the data were divided into a discovery dataset and a replication dataset. Only the discovery dataset was used for the present analyses (see Supplementary Table S2).

MRI data acquisition, processing and quality control

MRI data were collected at the Center for Translational Imaging at Northwestern University on a 3T Siemens Prisma scanner. A high-resolution T1-weighted magnetization-prepared rapid acquisition gradient echo (TR = 2,100 ms, TE = 2.9 ms, FOV = 256 mm, flip angle = 8°, slice thickness = 1 mm, 176 sagittal slices parallel to the AC-PC line) was acquired after the first resting-state run. Functional MRI were collected using a 64-channel head coil with a multi-band, multi-echo sequence with the following parameters: TR = 1,355 ms, TE = 12.80 ms, 32.39 ms, 51.98 ms, 71.57 ms, and 91.16 ms, flip angle = 64˚, voxel size = 2.4 mm, FOV = 216 mm x 216 mm, slice thickness = 2.4 mm, multiband slice acceleration factor = 6. Functional MRI data were pre-processed using the iProc pipeline[47] with the following steps. Runs with excessive head motion (a maximum FD > 0.2 mm or a maximum absolute displacement > 1 mm) were visually inspected and excluded if they exhibited noticeable movement. The first nine volumes (approximately 12 seconds) were removed to allow for T1 attenuation, and a mean BOLD template was generated using the remaining runs. Brain extraction was performed using FSL's Brain Extraction Tool (FSL v6.0.3). Nuisance signals relating to deep white matter, ventricular, and whole brain signal time series were regressed out of the data, followed by bandpass filtering at 0.01-0.10 Hz. Data were then projected onto a high-resolution standard surface mesh (fsaverage6, 40,962 vertices per hemisphere) using Freesurfer.[73] Finally, the data were spatially smoothed with a 2.5 mm full width-half maximum smoothing width, optimized to maintain precision while excluding noise. Pearson's product moment correlations were computed pairwise between vertices to generate a correlation matrix.

Clustering approach

The same MS-HBM parcellation method used for the 7T data was used to estimate networks [75] in the DBNO dataset.

Quantification and statistical analysis

Data from each participant (n = 6, NSD) were divided into a discovery dataset, for exploratory analysis, and replication and triplication datasets for validation (see Supplementary Table S1).

Seeds targeting each network in each cortical zone and individual were selected using the discovery dataset and used to extract timeseries for each run in the replication datasets in subjects that provided enough data (see *MRI data acquisition, processing and quality control*). Pearson's product-moment correlations were calculated between the extracted timeseries for each run in the replication dataset. We calculated correlations across all 34 seeds (5 seeds in each network except DN-A, which did not have an anterior insula seed), resulting in a 34 by 34 FC matrix for each run and each individual. The elements in these seed-wise FC matrices were then averaged together to generate network-network correlation values for each run. For within-network FC, we averaged only the lower triangle of the symmetric matrix to avoid repeats. A paired t-test was performed to compare within- versus between-network FC. Six separate t-tests (e.g., comparison between SAL/PMN vs. DN-A, SAL/PMN vs. DN-B, SAL/PMN vs. FPN-A, etc) were conducted for each target network. Benjamini-Hochberg correction was performed for the six comparisons. Following these individual-level analyses, we tested for consistency at the group level by averaging network-wise FC across sessions for each individual and then comparing within- versus between-network FC, as in the individual-level analyses. Additionally, n = 8 participants from an independent dataset (DBNO) were included in a replication analysis. For the seven participants with more than 10 good quality runs, the data were divided into a discovery dataset and a replication dataset. Only the discovery dataset was used for the present analyses (see Supplementary Table S2).

For task fMRI analysis, we performed two-tailed t-tests comparing each pair of trial types (P1, P2, and P3) to obtain a statistical map for each comparison of trial types. To control for the potential confounding effects of response time (RT), we included RT as a covariate.[78,79] Results did not differ considerably when RT was not modelled. All statistical analyses were conducted using FSL's Permutation Analysis of the Linear Model (PALM[80]) in MATLAB 2018b. To specifically test whether each cortical zone of SAL/PMN and other networks showed the repetition enhancement effect, we conducted three targeted analyses. First, we took the *a priori* defined seed vertices that were used in the statistical dissociation analyses (seeds shown in Supp. Figs. S2 & S3 and Figs. 2 & 3), calculated average trial-wise beta values at these vertices for each session for each trial type, and performed t-test for each contrast condition (P1 vs. P2, P1 vs. P3, and P2 vs. P3). Bonferroni correction was performed for the 3 comparisons. Second, we performed region-of-interest analysis by calculating the average betas across all vertices that were included as part of each network by the clustering analysis within 5 broad cortical regions: the posterior midline (encompassing PCU, RMC and rPCC), anterior midline (encompassing mPFC), the posterior lateral cortex (encompassing lPL), anterior lateral cortex (encompassing rPFC), and the anterior insula, and performed a two-sample t-test for each contrast condition (P1 vs. P2, P1 vs. P3, and P2 vs. P3). Bonferroni correction was performed for the 3 comparisons. Third, to focus on representative regions of SAL and PMN, located in mPFC and PCU/rPCC, respectively, and to determine whether the repetition effect is evident in both, we divided the SAL/PMN into posteromedial (canonical PMN) and anteromedial (canonical SAL) regions. Then we conducted a spin test (1,000 iterations) and compared observed t-values to null t-values obtained from the spin test to test statistical significance.[36,37] The division of the SAL/PMN into each component was done by hand-

drawing a large region of interest that bisected the midline along the caudal-rostral axis using Connectome Workbench (shown in Fig. 7B). The border was drawn from the top of the marginal sulcus to the most anterior part of the network in the rPCC, aiming to preserve contiguous canonical PMN (rPCC and PCU) and SAL (mPFC) regions in the midline. The border was drawn with reference to subject S6, whose rPCC SAL/PMN region was most anterior, and then applied to all the other subjects. The same analysis was repeated for the other six networks. Note that this line bisected a contiguous network region in CON-A and CON-B in some subjects. To test whether the repetition enhancement effect is observed in each region within each network, we averaged the *t*-values across all subjects and contrasts, and performed one-sample t-tests to assess the task effect.

Surface area analysis

To determine if a unified SAL/PMN better matches the surface area of all the other distributed networks, we calculated the percentage of total vertices in both hemispheres that were identified as belonging to each of network as a proxy for surface area. A one-way ANOVA was performed to assess differences across 7 intact (unified) networks. Next, we divided the SAL/PMN into anterior and posterior regions using the manually drawn region of interest used in the task spin permutation analysis. The region of interest was also extended along the lateral surface along the central sulcus, to bisect both the medial and lateral regions of SAL/PMN. We then performed another ANOVA across 8 networks (i.e., now including anterior SAL/PMN, posterior SAL/PMN, and the other 6 intact networks), followed by post-hoc pairwise comparisons using Tukey's Honestly Significant Difference test.

References

1. G. Doucet, M. Naveau, L. Petit, N. Delcroix, L. Zago, F. Crivello, G. Jobard, N. Tzourio-Mazoyer, B. Mazoyer, E. Mellet, M. Joliot, Brain activity at rest: a multiscale hierarchical functional organization. *J Neurophysiol*. **105**, 2753–2763 (2011).
2. P. S. Goldman-Rakic, Topography of cognition: parallel distributed networks in primate association cortex. *Annual Review of Neuroscience*. **11**(1), 137-156 (1988).
3. J. D. Power, A. L. Cohen, S. M. Nelson, G. S. Wig, K. A. Barnes, J. A. Church, A. C. Vogel, T. O. Laumann, F. M. Miezin, B. L. Schlaggar, S. E. Petersen, Functional Network Organization of the Human Brain. *Neuron*. **72**(4), 665–678 (2011).
4. S. M. Smith, P. T. Fox, K. L. Miller, D. C. Glahn, P. M. Fox, C. E. Mackay, N. Filippini, K. E. Watkins, R. Toro, A. R. Laird, C. F. Beckmann, Correspondence of the brain's functional architecture during activation and rest. *Proceedings of the National Academy of Sciences of the United States of America*. **106**(31), 13040–13045 (2009).
5. B. T. Yeo, F. M. Krienen, J. Sepulcre, M. R. Sabuncu, D. Lashkari, M. Hollinshead, J. L. Roffman, J. W. Smoller, L. Zöllei, J. R. Polimeni, B. Fisch, H. Liu, R. L. Buckner, The organization of the human cerebral cortex estimated by intrinsic functional connectivity. *Journal of Neurophysiology*, **106**(3), 1125–1165 (2011).
6. N. Kanwisher, Functional specificity in the human brain: a window into the functional architecture of the mind. *Proceedings of the national academy of sciences*. **107**(25), 11163-11170 (2010).

7. L. Krubitzer, The magnificent compromise: cortical field evolution in mammals. *Neuron*. **56**(2), 201–208 (2007).
8. D. S. Margulies, S. S. Ghosh, A. Goulas, M. Falkiewicz, J. M. Huntenburg, G. Langs, G. Bezgin, S. B. Eickhoff, F. X. Castellanos, M. Petrides, E. Jefferies, J. Smallwood, Situating the default-mode network along a principal gradient of macroscale cortical organization. *Proceedings of the National Academy of Sciences*, **113**(44), 12574-12579 (2016).
9. L. R. Squire, Mechanisms of Memory. Science. **232**(4758), 1612–1619 (1986).
10. R. Cabeza, E. Ciaramelli, I. R. Olson, M. Moscovitch, The parietal cortex and episodic memory: an attentional account. *Nature reviews neuroscience*. **9**(8), 613-625 (2008).
11. A. P. Yonelinas, L. J. Otten, K. N. Shaw, M. D. Rugg, Separating the brain regions involved in recollection and familiarity in recognition memory. *Journal of Neuroscience*. **25**(11), 3002-3008 (2005).
12. A. P. Yonelinas, J. Scheib, N. Kroll, M. Lazzara, J. Quamme, M. Kishiyama, E. Nolan, T. Jacobs, C. Brozin-Sky, C. Ranganath, P. Yonelinas, The Nature of Recollection and Familiarity: A Review of 30 Years of Research. *Journal of Memory and Language*. **46**, 441–517 (2002).
13. H. Y. Chen, A. W. Gilmore, S. M. Nelson, K. B. McDermott, Are There Multiple Kinds of Episodic Memory? An fMRI Investigation Comparing Autobiographical and Recognition Memory Tasks. *Journal of Neuroscience*. **37**(10), 2764-2775 (2017).
14. M. E. Wheeler, R. L. Buckner, Functional-anatomic correlates of remembering and knowing. *Neuroimage*. **21**(4), 1337-1349 (2004).
15. D. R. Addis, A. T. Wong, D. L. Schacter, Remembering the past and imagining the future: Common and distinct neural substrates during event construction and elaboration. *Neuropsychologia*, **45**, 1363–1377 (2007).
16. R. L. Buckner, J. R. Andrews-Hanna, D. L. Schacter, The Brain's Default Network. *Annals of the New York Academy of Sciences*, **1124**(1), 1–38 (2008).
17. L. M. DiNicola, R. M. Braga, R. L. Buckner, Parallel distributed networks dissociate episodic and social functions within the individual. *Journal of Neurophysiology*. **123**(3), 1144–1179 (2020).
18. A. D. Wagner, B. J. Shannon, I. Kahn, R. L. Buckner, Parietal lobe contributions to episodic memory retrieval. *Trends in cognitive sciences*. **9**(9), 445-453 (2005).
19. J. L. Vincent, A. Z. Snyder, M. D. Fox, B. J. Shannon, J. R. Andrews, M. E. Raichle, R. L. Buckner, Coherent spontaneous activity identifies a hippocampal-parietal memory network. *Journal of Neurophysiology*. **96**(6), 3517–3531 (2006).
20. L. M. DiNicola, O. I. Ariyo, R. L. Buckner, Functional specialization of parallel distributed networks revealed by analysis of trial-to-trial variation in processing demands. *Journal of Neurophysiology*. **129**(1), 17–40 (2023).
21. M. Peer, R. Salomon, I. Goldberg, O. Blanke, S. Arzy, Brain system for mental orientation in space, time, and person. *Proceedings of the National Academy of Sciences of the United States of America*. **112**(35), 11072–11077 (2015).
22. E. H. Silson, A. Steel, A. Kidder, A. W. Gilmore, C. I. Baker, Distinct subdivisions of human medial parietal cortex support recollection of people and places. *ELife*. **8** (2019).

23. A. W. Gilmore, S. M. Nelson, K. B. McDermott, A parietal memory network revealed by multiple MRI methods. *Trends in Cognitive Sciences*. **19**(9), 534–543 (2015).
24. A. W. Gilmore, S. M. Nelson, T. O. Laumann, E. M. Gordon, J. J. Berg, D. J. Greene, C. Gratton, A. L. Nguyen, M. Ortega, C. R. Hoyt, R. S. Coalson, B. L. Schlaggar, S. E. Petersen, N. U. F. Dosenbach, K. B. McDermott, High-fidelity mapping of repetition-related changes in the parietal memory network. *NeuroImage*. **199**, 427–439 (2019).
25. H. Kim, Brain regions that show repetition suppression and enhancement: A meta-analysis of 137 neuroimaging experiments. *Human Brain Mapping*. **38**(4), 1894 (2017).
26. K. Segaert, K. Weber, F. P. de Lange, K. M. Petersson, P. Hagoort, The suppression of repetition enhancement: a review of fMRI studies. *Neuropsychologia*. **51**(1), 59-66 (2013).
27. M. L. Rosen, C. E. Stern, K. J. Devaney, D. C. Somers, Cortical and Subcortical Contributions to Long-Term Memory-Guided Visuospatial Attention. *Cerebral Cortex*. **28**, 2935–2947 (2018).
28. R. M. Braga, R. L. Buckner, Parallel Interdigitated Distributed Networks within the Individual Estimated by Intrinsic Functional Connectivity. *Neuron*. 95(2), 457-471.e5 (2017).
29. L. M. DiNicola, R. L. Buckner, Precision estimates of parallel distributed association networks: evidence for domain specialization and implications for evolution and development. *Current Opinion in Behavioral Sciences*. **40**, 120–129 (2021).
30. J. Du, L. M. DiNicola, P. A. Angeli, N. Saadon-Grosman, W. Sun, S. Kaiser, J. Ladopoulou, A. Xue, B. T. T. Yeo, M. C. Eldaief, R. L. Buckner, Organization of the Human Cerebral Cortex Estimated Within Individuals: Networks, Global Topography, and Function. *Journal of Neurophysiology*. (2024).
31. H. L. Kosakowski, M. C. Eldaief, R. L. Buckner, Ventral Striatum is Preferentially Correlated with the Salience Network Including Regions in Dorsolateral Prefrontal Cortex. *bioRxiv*. 10.1101/2024.10.13.618063 (2024).
32. D. Reznik, D. S. Margulies, M. P. Witter, C. F. Doeller, Evidence for convergence of distributed cortical processing in band-like functional zones in human entorhinal cortex. *Current Biology*. **34**, 1-13 (2024).
33. P. A. Angeli, L. M. DiNicola, N. Saadon-Grosman, M. C. Eldaief, R. L. Buckner, Specialization of the Human Hippocampal Long Axis Revisited. *bioRxiv.* 10.1101/2023.12.19.572264 (2023).
34. A. W. Gilmore, S. M. Nelson, K. B. McDermott, Precision functional mapping of human memory systems. *Current Opinion in Behavioral Sciences*. **40**, 52-57 (2021).
35. A. Schaefer, R. Kong, E. M. Gordon, T. O. Laumann, X.-N. Zuo, A. J. Holmes, S. B. Eickhoff, B. T. T. Yeo, Local-Global Parcellation of the Human Cerebral Cortex from Intrinsic Functional Connectivity MRI. *Cerebral Cortex*. **28**(9), 3095–3114 (2018).
36. E. M. Gordon, T. O. Laumann, B. Adeyemo, J. F. Huckins, W. M. Kelley, S.E. Petersen, Generation and evaluation of a cortical area parcellation from resting-state correlations. *Cerebral cortex*. **26**(1), 288-303 (2016).
37. E. M. Gordon, T. O. Laumann, A. W. Gilmore, D. J. Newbold, D. J. Greene, J. J. Berg, M. Ortega, C. Hoyt-Drazen, C. Gratton, H. Sun, J. M. Hampton, R. S. Coalson, A. L. Nguyen, K. B. McDermott, J. S. Shimony, A. Z. Snyder, B. L. Schlaggar, S. E.

Petersen, S. M. Nelson, N. U. F. Dosenbach, Precision Functional Mapping of Individual Human Brains. *Neuron*. **95**(4), 791-807.e7 (2017).
38. R. Kong, J. Li, C. Orban, M. R. Sabuncu, H. Liu, A. Schaefer, N. Sun, X. N. Zuo, A. J. Holmes, S. B. Eickhoff, B. T. T. Yeo, Spatial Topography of Individual-Specific Cortical Networks Predicts Human Cognition, Personality, and Emotion. *Cerebral Cortex*. **29**(6), 2533–2551 (2019).
39. W. R. Shirer, S. Ryali, E. Rykhlevskaia, V. Menon, M. D. Greicius, Decoding Subject-Driven Cognitive States with Whole-Brain Connectivity Patterns. *Cerebral Cortex*. **22**(1), 158–165 (2012).
40. H. Kim, Differential neural activity in the recognition of old versus new events: An Activation Likelihood Estimation Meta-Analysis. *Human Brain Mapping*. **34**(4), 814–836 (2013).
41. K. B. McDermott, K. K. Szpunar, S. E. Christ, Laboratory-based and autobiographical retrieval tasks differ substantially in their neural substrates. *Neuropsychologia*. **47**(11), 2290–2298 (2009).
42. L. J. Otten, M. D. Rugg, Task-dependency of the neural correlates of episodic encoding as measured by fMRI. *Cerebral cortex*. **11**(12), 1150-1160 (2001).
43. J. Chen, Y. C. Leong, C. J. Honey, C. H. Yong, K. A. Norman, U. Hasson, Shared memories reveal shared structure in neural activity across individuals. *Nature neuroscience*, **20**(1), 115-125 (2017).
44. T. O. Laumann, E. M. Gordon, B. Adeyemo, A. Z. Snyder, S. J. Joo, M. Y. Chen, A. W. Gilmore, K. B. McDermott, S. M. Nelson, N. U. F. Dosenbach, B. L. Schlaggar, J. A. Mumford, R. A. Poldrack, S. E. Petersen, Functional System and Areal Organization of a Highly Sampled Individual Human Brain. *Neuron*. **87**(3), 657–670 (2015).
45. R. A. Poldrack, T. O. Laumann, O. Koyejo, B. Gregory, A. Hover, M. Y. Chen, K. J. Gorgolewski, J. Luci, S. J. Joo, R. L. Boyd, S. Hunicke-Smith, Z. B. Simpson, T. Caven, V. Sochat, J. Shine, E. M. Gordon, A. Z. Snyder, B. Adeyemo, S. E. Petersen, D. C. Glahn, D. R. Mckay, J. E. Curran, H. H. H. Goring, M. A. Carless, J. Blangero, R. Dougherty, A. Leemans, D. A. Handwerker, L. Frick, E. M. Marcotte, J. A. Mumford, Long-term neural and physiological phenotyping of a single human. *Nature communications*. **6**, 8885 (2015).
46. R. M. Braga, L. M. DiNicola, H. C. Becker, R. L. Buckner, Situating the left-lateralized language network in the broader organization of multiple specialized large-scale distributed networks. *Journal of Neurophysiology*. **124**(5), 1415–1448 (2020).
47. R. M. Braga, K. R. A. Van Dijk, J. R. Polimeni, M. C. Eldaief, R. L. Buckner, Parallel distributed networks resolved at high resolution reveal close juxtaposition of distinct regions. *Journal of Neurophysiology*. **121**(4), 1513–1534 (2019).
48. E. M. Gordon, R. J. Chauvin, A. N. Van, A. Rajesh, A. Nielsen, D. J. Newbold, C. J. Lynch, N. A. Seider, S. R. Krimmel, K. M. Scheidter, J. Monk, R. L. Miller, A. Metoki, D. F. Montez, A. Zheng, I. Elbau, T. Madison, T. Nishino, M. J. Myers, S. Kaplan, C. B. D'Andrea, D. V. Demeter, M. Feigelis, J. S. B. Ramirez, T. Xu, D. M. Barch, C. D. Smyser, C. E. Rogers, J. Zimmermann, K. N. Botteron, J. R. Pruett, J. T. Willie, P. Brunner, J. S. Shimony, B. P. Kay, S. Marek, S. A. Norris, C. Gratton, C. M. Sylvester, J. D. Power, C. Liston, D. J. Greene, J. L. Roland, S. E. Petersen, M. E. Raichle, T. O.

Laumann, D. A. Fair, N. U. F. Dosenbach, A somato-cognitive action network alternates with effector regions in motor cortex. *Nature*, **617** (2023).
49. D. J. Newbold, T. O. Laumann, C. R. Hoyt, J. M. Hampton, D. F. Montez, R. V. Raut, M. Ortega, A. Mitra, A. N. Nielsen, D. B. Miller, B. Adeyemo, A. L. Nguyen, K. M. Scheidter, A. B. Tanenbaum, A. N. Van, S. Marek, B. L. Schlaggar, A. R. Carter, D. J. Greene, E. M. Gordon, M. E. Raichle, S. E. Petersen, A. Z. Snyder, N. U. F. Dosenbach, Plasticity and spontaneous activity pulses in disused human brain circuits. *Neuron*, **107**(3), 580-589 (2020).
50. B. A. Seitzman, C. Gratton, T. O. Laumann, E. M. Gordon, B. Adeyemo, A. Dworetsky, B. T. Kraus, A. W. Gilmore, J. J. Berg, M. Ortega, A. Nguyen, D. J. Greene, K. B. McDermott, S. M. Nelson, C. N. Lessov-Schlaggar, B. L. Schlaggar, N. U. F. Dosenbach, S. E. Petersen, Trait-like variants in human functional brain networks. *Proceedings of the National Academy of Sciences*, **116**(45), 22851-22861 (2019).
51. A. Zheng, D. F. Montez, S. Marek, A. W. Gilmore, D. J. Newbold, T. O. Laumann, B. P. Kay, N. A. Seider, A. N. Van, J. M. Hampton, D. Alexopoulos, B. L. Schlaggar, C. M. Sylvester, D. J. Greene, J. S. Shimony, S. M. Nelson, G. S. Wig, C. Gratton, K. B. McDermott, M. E. Raichle, E. M. Gordon, N. U. F. Dosenbach, Parallel hippocampal-parietal circuits for self-and goal-oriented processing. *Proceedings of the National Academy of Sciences*, **118**(34), e2101743118 (2021).
52. C. Amiez, M. G. Wutte, I. Faillenot, M. Petrides, B. Burle, E. Procyk, Single subject analyses reveal consistent recruitment of frontal operculum in performance monitoring. *Neuroimage*. **133**, 266-278 (2016).
53. N. U. Dosenbach, M. Raichle, E.M. Gordon, The brain's cingulo-opercular action-mode network. *PsyArXiv*. 10.31234/osf.io/2vt79 (2024).
54. C. J. Lynch, I. G. Elbau, T. Ng, A. Ayaz, S. Zhu, D. Wolk, N. Manfredi, M. Johnson, M. Chang, J. Chou, I. Summerville, C. Ho, M. Lueckel, H. Bukhari, D. Buchanan, L. W. Victoria, N. Solomonov, E. Goldwaser, S. Moia, C. Caballero-Gaudes, J. Downar, F. Vila-Rodriguex, Z.J. Daskalakis, D.M. Blumberger, K. Kay, A. Aloysi, E. M. Gordon, M. T. Bhati, N. Williams, J. D. Power, B. Zebley, L. Grosenick, F. M. Gunning, C. Liston. Frontostriatal salience network expansion in individuals in depression. *Nature*. **633**, 624–633 (2024).
55. W. W. Seeley, The salience network: a neural system for perceiving and responding to homeostatic demands. *Journal of Neuroscience*. **39**(50), 9878-9882 (2019).
56. K. L. Miller, F. Alfaro-Almagro, N. K. Bangerter, D. L. Thomas, E. Yacoub, J. Xu, A. J. Bartsch, S. Jbabdi, S. N. Sotiropoulos, J. L. R. Andersson, L. Griffanti, G. Douaud, T. W. Okell, P. Weale, I. Dragonu, S. Garratt, S. Hudson, R. Collins, M. Jenkinson, P. M. Matthews, S. M. Smith, Multimodal population brain imaging in the UK Biobank prospective epidemiological study. *Nature neuroscience*. **19**(11), 1523-1536 (2016)
57. E. M. Gordon, T. O. Laumann, S. Marek, D. J. Newbold, J. M. Hampton, N. A. Seider, D. F. Montez, A. M. Nielsen, A. N. Van, A. Zheng, R. Miller, J. S. Siegel, B. P. Kay, A. Z. Snyder, D. J. Greene, B. L. Schlaggar, S. E. Petersen, S. M. Nelson, N. U. F. Dosenbach, Individualized functional subnetworks connect human striatum and frontal cortex. *Cerebral Cortex*. **32**(13), 2868-2884 (2022).

58. D. Edmonds, J. J. Salvo, N. Anderson, M. Lakshman, Q. Yang, K. Kay, C. Zelano, R. M. Braga, The human social cognitive network contains multiple regions within the amygdala. *Science Advances*, 10(47), eadp0453 (2024).
59. C. B. D'Andrea, T. O. Laumann, D. J. Newbold, S. M. Nelson, A. N. Nielsen, R. Chauvin, S. Marek, D. J. Greene, N. U. F. Dosenbach, E. M. Gordon, Substructure of the brain's Cingulo-Opercular network. *bioRxiv*. 10.1101/2023.10.10.561772 (2023).
60. Gratton, C., Dworetsky, A., Adeyemo, B., Seitzman, B. A., Smith, D. M., Petersen, S. E., & Neta, M. The cingulo-opercular network is composed of two distinct sub-systems. *bioRxiv*. 10.1101/2022.09.16.508254 (2022).
61. E. M. Gordon, T. O. Laumann, B. Adeyemo, A. W. Gilmore, S. M. Nelson, N. U. F. Dosenbach, S. E. Petersen, Individual-specific features of brain systems identified with resting-state functional correlations. *Neuroimage*. **146**, 918-939 (2017).
62. S. M. Nelson, K. M. Arnold, A. W. Gilmore, K. B. McDermott, Neural Signatures of Test-Potentiated Learning in Parietal Cortex. *Journal of Neuroscience*. **33**(29), 11754–11762 (2013).
63. R. L. Buckner, F. M. Krienen, The evolution of distributed association networks in the human brain. *Trends in Cognitive Sciences*. **17**(12), 648–665 (2013).
64. S. Mueller, D. Wang, M. D. Fox, B. T. Yeo, J. Sepulcre, M. R. Sabuncu, R. Shafee, J. Lu, H. Liu, Individual variability in functional connectivity architecture of the human brain. Neuron. 77(3), 586-95 (2013).
65. A. Dworetsky, B. A. Seitzman, B. Adeyemo, A. N. Nielsen, A. S. Hatoum, D. M. Smith, T. E. Nichols, M. Neta, S. E. Petersen, C. Gratton, Two common and distinct forms of variation in human functional brain networks. *Nature Neuroscience*. **27**, 1187-1198 (2024).
66. N. U. Dosenbach, K. M. Visscher, E. D. Palmer, F. M. Miezin, K. K. Wenger, H. C. Kang, E. D. Burgund, A. L. Grimes, B. L. Schlaggar, S. E. Petersen, A core system for the implementation of task sets. *Neuron*. **50**(5), 799-812 (2006).
67. Z. Cui, H. Li, C. H. Xia, B. Larsen, A. Adebimpe, G. L. Baum, M. Cieslak, R. E. Gur, R. C. Gur, T. M. Moore, D. J. Oathes, A. F. Alexander-Bloch, A. Raznahan, D. R. Roalf, R. T. Shinohara, D. H. Wolf, C. Davatzikos, D. S. Bassett, D. A. Fair, Y. Fan, T. D. Satterthwaite, Individual variation in functional topography of association networks in youth. *Neuron*. **106**(2), 340-53 (2020).
68. W. Qiu, L. Ma, T. Jiang, Y. Zhang. Unrevealing reliable cortical parcellation of individual brains using resting-state functional magnetic resonance imaging and masked graph convolutions. *Frontiers in Neuroscience*. **16**, 838347 (2022).
69. M. D. Fox, A. Z. Snyder, J. L. Vincent, M. Corbetta, D. C. Van Essen, M. E. Raichle, The human brain is intrinsically organized into dynamic, anticorrelated functional networks. *Proceedings of the National Academy of Sciences of the United States of America*. **102**(27), 9673–9678 (2005).
70. J. D. Bijsterbosch, S. R. Farahibozorg, M. F. Glasser, D. Van Essen, L. H. Snyder, M. W. Woolrich, S. M. Smith, Evaluating functional brain organization in individuals and identifying contributions to network overlap. *Imaging Neuroscience*. **1**, 1-19, (2023).
71. E. J. Allen, G. St-Yves, Y. Wu, J. L. Breedlove, J. S. Prince, L. T. Dowdle, M. Nau, B. Caron, F. Pestilli, I. Charest, J. B. Hutchinson, T. Naselaris, K. Kay, A massive 7T fMRI

dataset to bridge cognitive neuroscience and artificial intelligence. *Nature Neuroscience*. **25**(1), 116-126 (2021).
72. R. W. Cox, AFNI: Software for Analysis and Visualization of Functional Magnetic Resonance Neuroimages. *Computers and Biomedical Research*. **29**(3), 162–173 (1996).
73. B. Fischl, M. I. Sereno, A. M. Dale, Cortical Surface-Based Analysis: II: Inflation, Flattening, and a Surface-Based Coordinate System. *NeuroImage*. 9(2), 195–207 (1999).
74. D. S. Marcus, J. Harwell, T. Olsen, M. Hodge, M. F. Glasser, F. Prior, M. Jenkinson, T. Laumann, S. W. Curtiss, D. C. Van Essen, Informatics and data mining tools and strategies for the human connectome project. *Frontiers in neuroinformatics*. **5**, 4 (2011).
75. R. Kong, Q. Yang, E. Gordon, A. Xue, X. Yan, C. Orban, X.-N. Zuo, N. Spreng, T. Ge, A. Holmes, S. Eickhoff, B. T. T. Yeo, Individual-Specific Areal-Level Parcellations Improve Functional Connectivity Prediction of Behavior. Cerebral Cortex. 31(10) (2021).
76. S. M. Smith, M. Jenkinson, M. W. Woolrich, C. F. Beckmann, T. E. J. Behrens, H. Johansen-Berg, P. R. Bannister, M. De Luca, I. Drobnjak, D. E. Flitney, R. K. Niazy, J. Saunders, J. Vickers, Y. Zhang, N. De Stefano, J. M. Brady, P. M. Matthews, Advances in functional and structural MR image analysis and implementation as FSL. NeuroImage 23, S208–S219 (2004).
77. H. J. Jo, Z. S. Saad, W. K. Simmons, L. A. Milbury, R. W. Cox, Mapping sources of correlation in resting state FMRI, with artifact detection and removal. *NeuroImage.* **52**, 571–582 (2010).
78. J. S. H. Taylor, K. Rastle, M. H. Davis, Interpreting response time effects in functional imaging studies. *NeuroImage*. **99**, 419–433 (2014).
79. T. Yarkoni, D. M. Barch, J. R. Gray, T. E. Conturo, T. S. Braver, BOLD Correlates of Trial-by-Trial Reaction Time Variability in Gray and White Matter: A Multi-Study fMRI Analysis. *PLOS ONE*. **4**(1), e4257 (2009).
80. A. M. Winkler, G. R. Ridgway, G. Douaud, T. E. Nichols, S. M. Smith, Faster permutation inference in brain imaging. *NeuroImage*. **141**, 502–516 (2016).

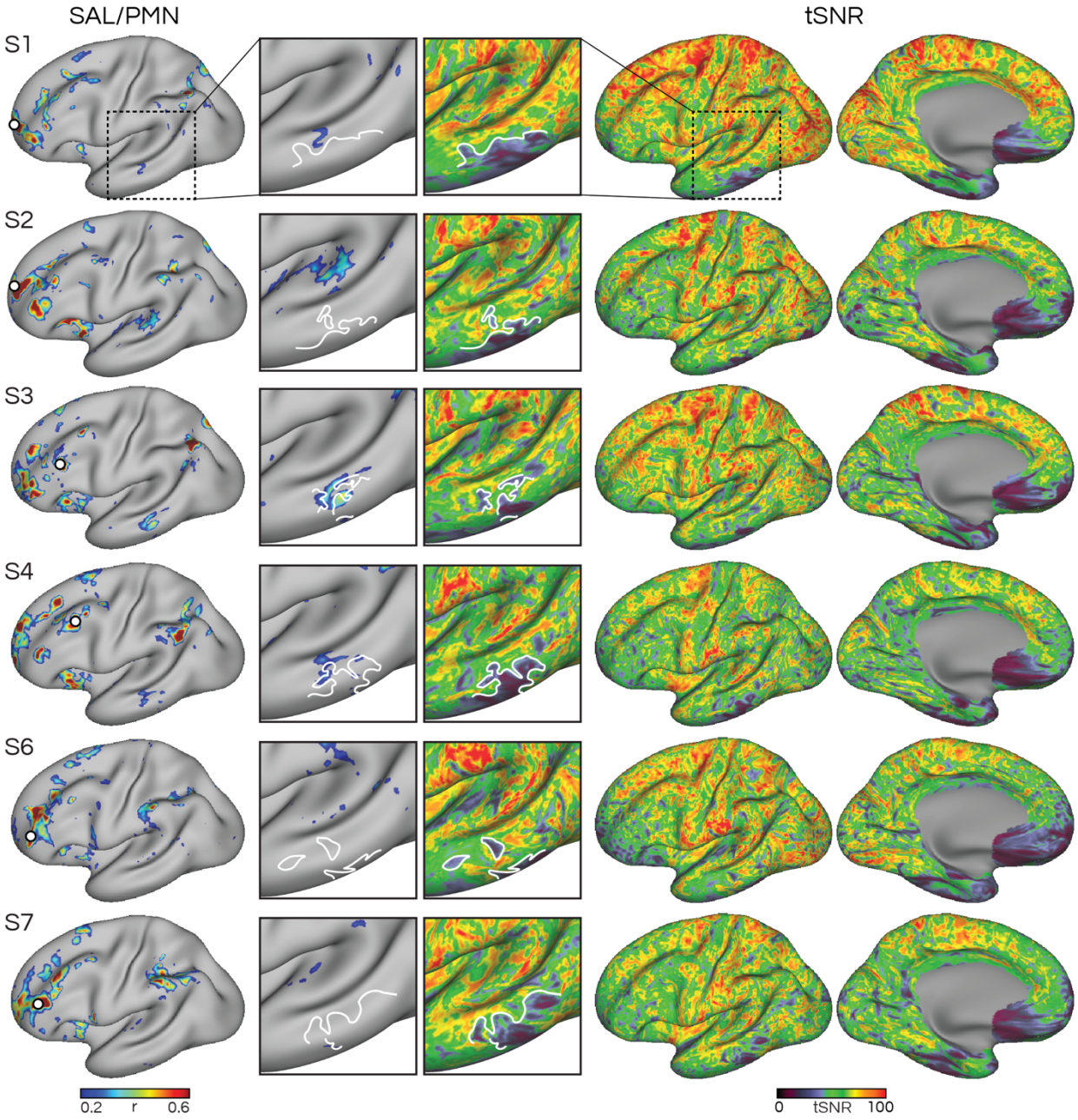

Supp. Fig. S1: Good data quality was achieved in the high-resolution 7T Natural Scenes Dataset, but signal dropout may have affected detection of a salience/parietal memory network (SAL/PMN) region in the lateral temporal cortex, Related to Fig. 4. The left columns show the functional connectivity map of the SAL/PMN defined using a seed-based approach (seeds shown as white circles), and the right columns show the temporal signal-to-noise ratio (tSNR) maps for all six NSD participants (rows). The tSNR maps show that good data quality and coverage was achieved by the high-field 7T protocol, despite the small voxel size (1.8 mm isotropic). Signal dropout regions (cooler colors) can be seen in the temporal pole, lateral temporal cortex, and ventromedial prefrontal cortex. Insets show a zoom-in of the lateral temporal cortex. The white lines trace the idiosyncratic shape of vertices affected by signal dropout in each individual. In 3 subjects (S1, S3, S4), evidence for a region of the SAL/PMN was detected in close proximity to the dropout, raising the prospect that a lateral temporal SAL/PMN region may have been missed in the other participants. Analysis of UK Biobank data containing 4,181 participants also suggested the presence of this SAL/PMN region (see Fig. 4C).

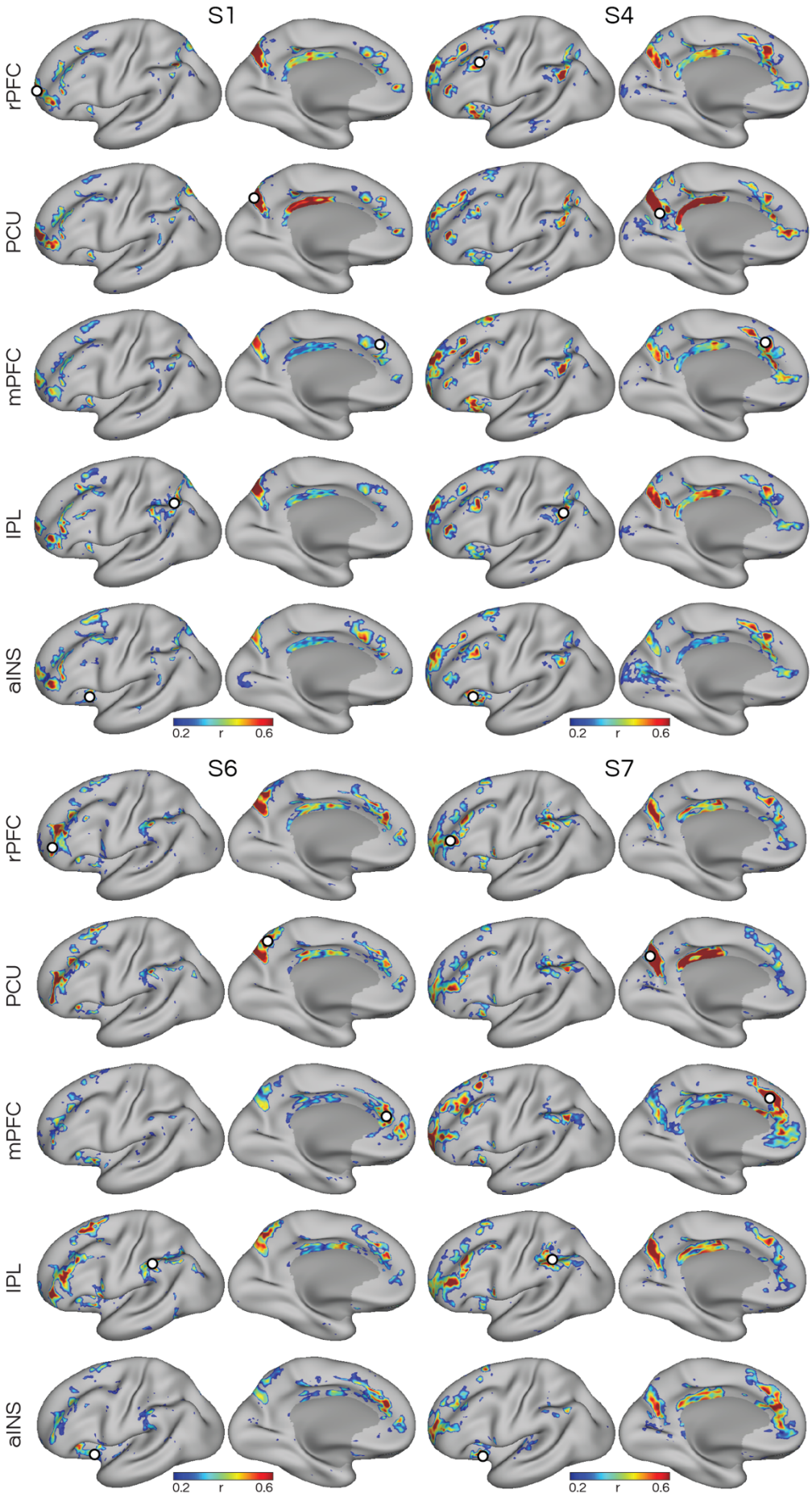
S1
S4
S6
S7
rPFC
PCU
mPFC
IPL
aINS
0.2
r
0.6

Supp. Fig. S2: Seed-based functional connectivity at high resolution reproducibly defines the SAL/PMN in multiple cortical zones, Related to Fig. 2, reinforcing that the SAL/PMN is a distributed association network. Five estimates of the SAL/PMN are shown in four participants (with the remaining two subjects shown in Fig. 2). Seeds (white circles) were selected from five cortical zones, including the rostral prefrontal cortex (rPFC), posteromedial cortex (including precuneus; PCU), medial prefrontal cortex (mPFC), inferior parietal lobule (IPL), and anterior insula (aINS). Note that differences between the seeds are expected, as correlation values are inflated near the seed. Despite these differences, each of the seeds replicate a similar distribution of regions.

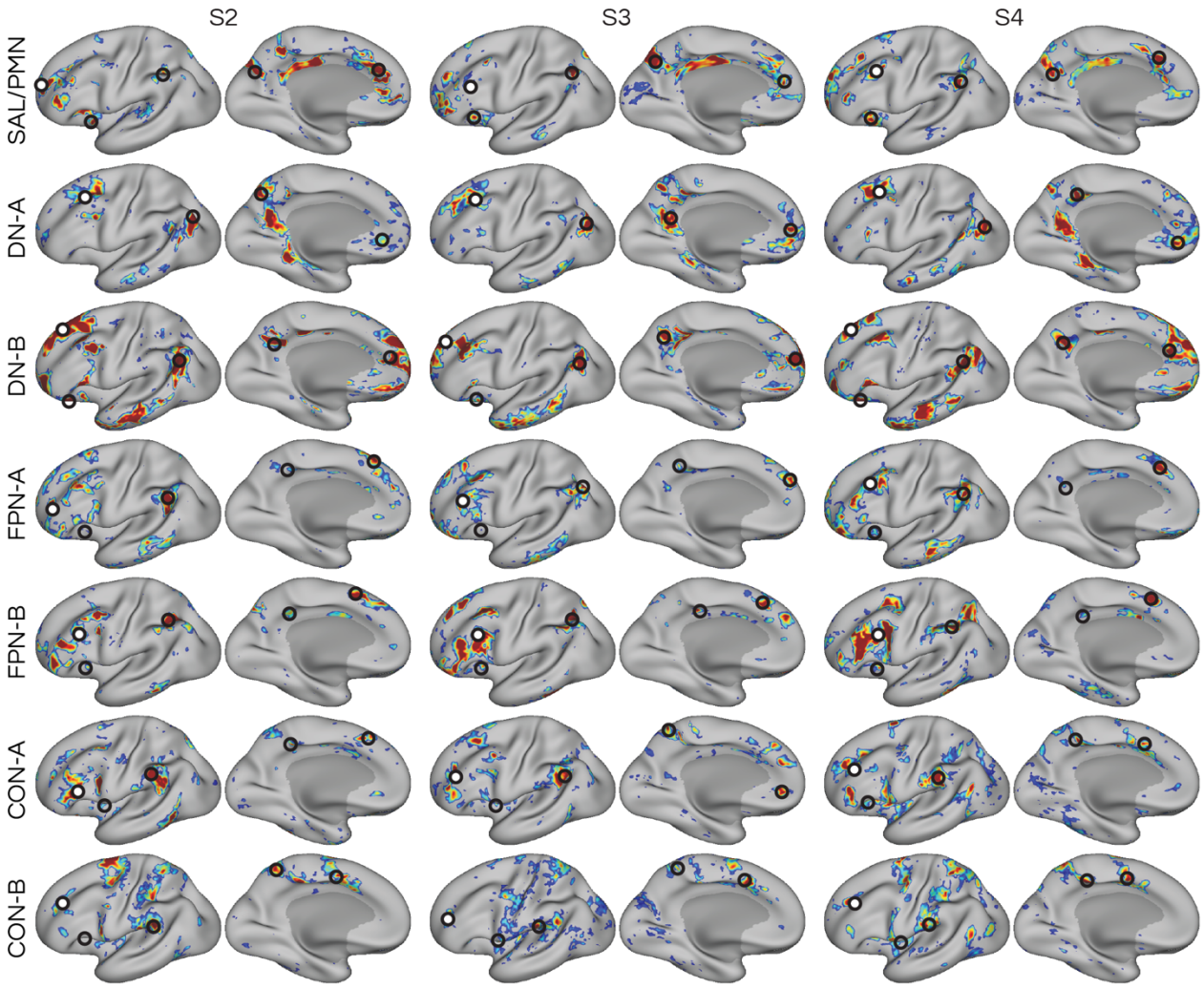

Supp. Fig. S3: Seed-based network estimation confirms the SAL/PMN is distinct from nearby distributed networks, Related to Fig. 3. Seeds were initially selected from the rostral prefrontal cortex (white circles) in each individual (S2, S3 & S4 shown here as examples) targeting seven distributed networks (rows): the SAL/PMN, default network A (DN-A), default network B (DN-B), frontoparietal network A (FPN-A), frontoparietal network B (FPN-B), cingulo-opercular network A (CON-A), and cingulo-opercular network B (CON-B). Next, seeds (black hollow circles) were selected targeting regions of each network in four other cortical zones (anterior insula, inferior parietal lobule, precuneus, medial prefrontal cortex) for the statistical dissociation analyses in Fig. 3. One exception was DN-A which only contained 3 zones as the network did not display an insula region.

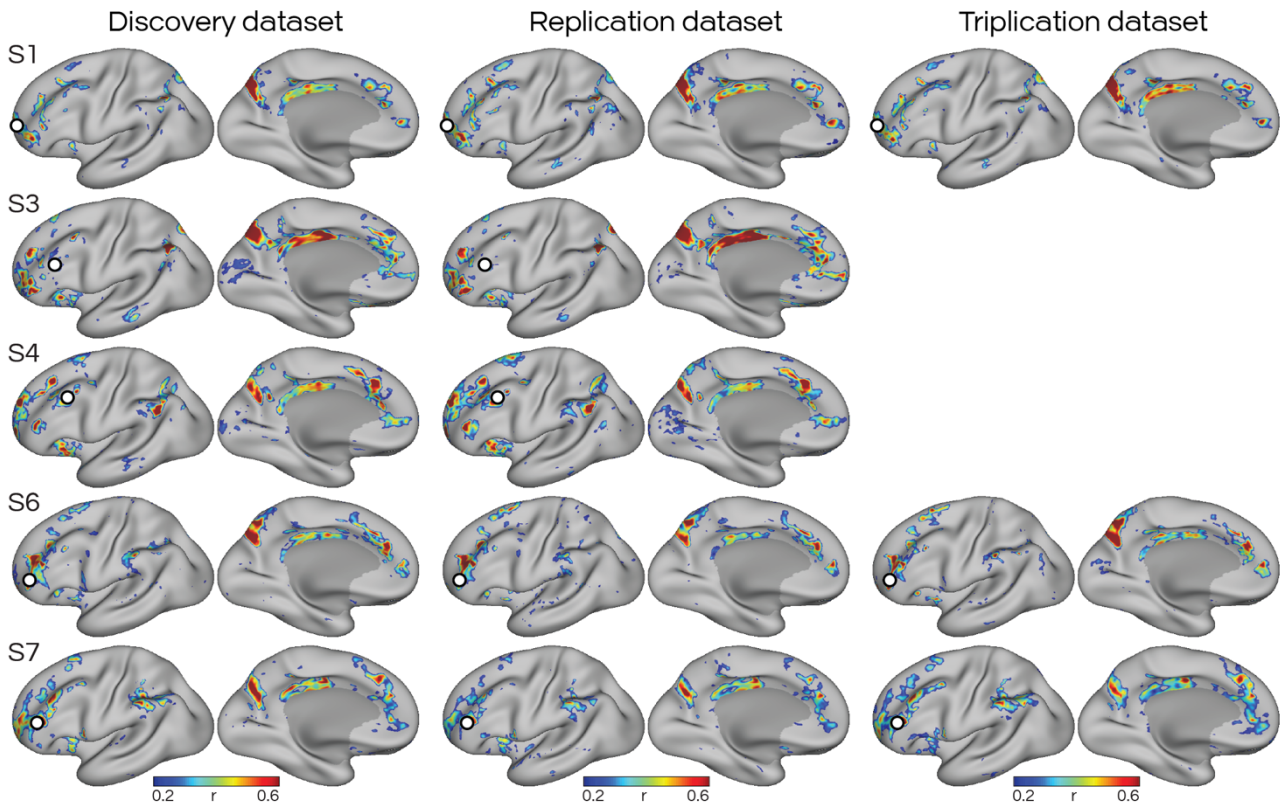

Supp. Fig. S4: The distributed organization of SAL/PMN is replicated and triplicated in the left-out data, Related to Fig. 3. Once statistical analysis had been run in the left-out validation data (Fig. 3), the seeds selected from the discovery dataset (white circles) were applied to the left-out datasets in each subject for replication and triplication. The estimates demonstrate that SAL/PMN reproducibly includes regions distributed throughout multiple cortical zones, including medial prefrontal and anterior insula.

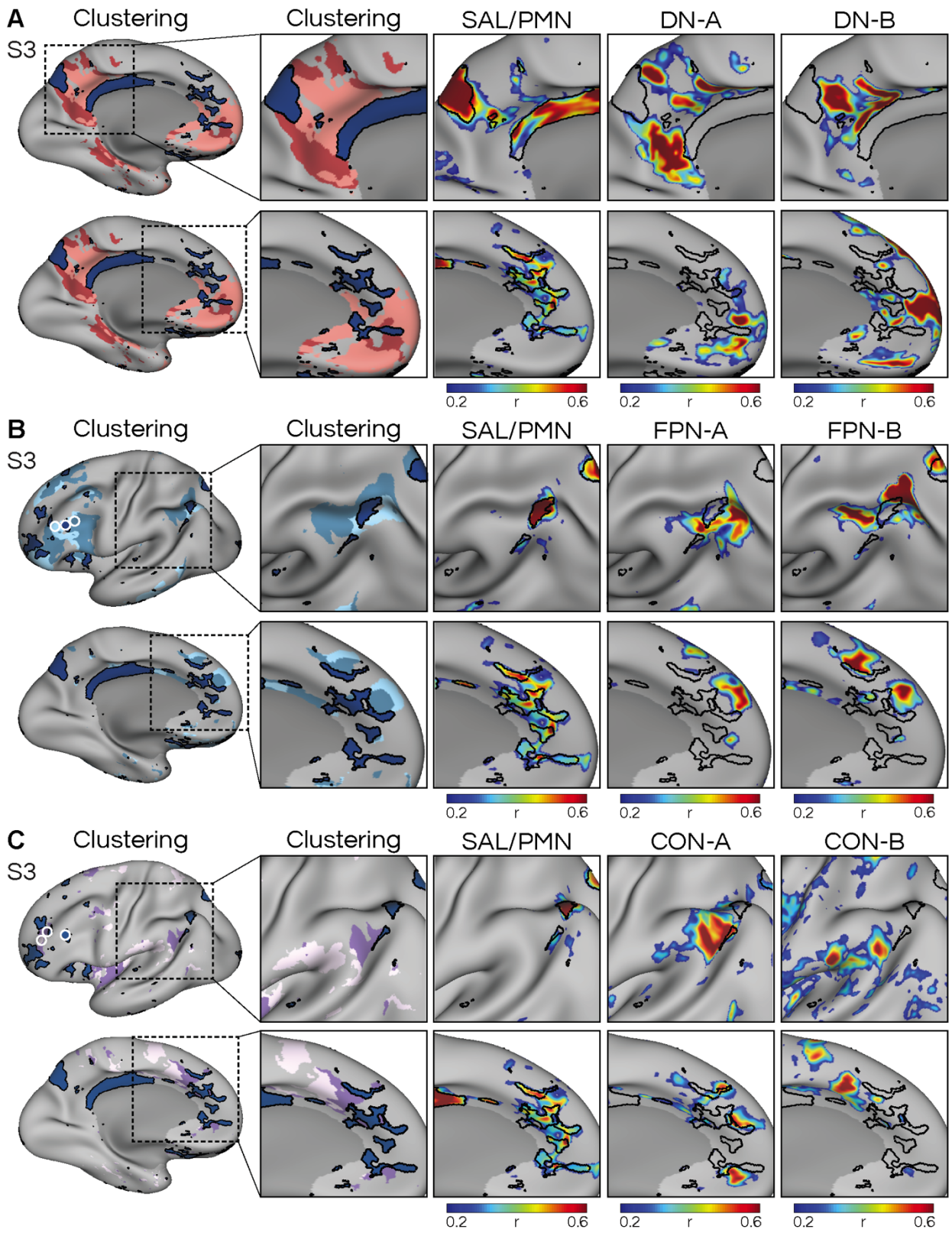

Supp. Fig. S5: Detailed anatomy reveals that SAL/PMN regions are interdigitated with but distinct from networks within the canonical default (DN), frontoparietal control (FPN), and cingulo-opercular (CON) networks, Related to Fig. 1, 2, and 3. A. Left column shows the clustering-defined networks from Fig. 1 and the location of manually selected seeds (white circles) initially used to define the networks. The full seed-based maps from these seeds are shown in Supp. Fig. S3. A representative participant (S3) is shown, with the remaining 5 shown in Supp. Fig. S6. Right insets show a zoom-in of the posteromedial (top row) and

anteromedial (bottom) cortex of clustering (1st inset) and seed-based estimates of each network (remaining insets) to highlight that the correlated regions of SAL/PMN occupy distinct patches of the cortical mantle compared to DN-A and DN-B. The black lines represent the boundaries of the SAL/PMN calculated from the clustering approach, to serve as landmarks for comparing across panels. **B.** Insets show a zoom-in of the intraparietal sulcus (top row; zoom-in insets are rotated for better visualization within the intraparietal sulcus) and medial prefrontal cortex (bottom) showing the distinction between SAL/PMN and FPN-A and FPN-B. **C.** Insets show a zoom-in of the intraparietal sulcus (top) and medial prefrontal cortex (bottom) comparing SAL/PMN and CON-A and CON-B. The remaining five participants are shown in Supp. Fig. S7—S8.

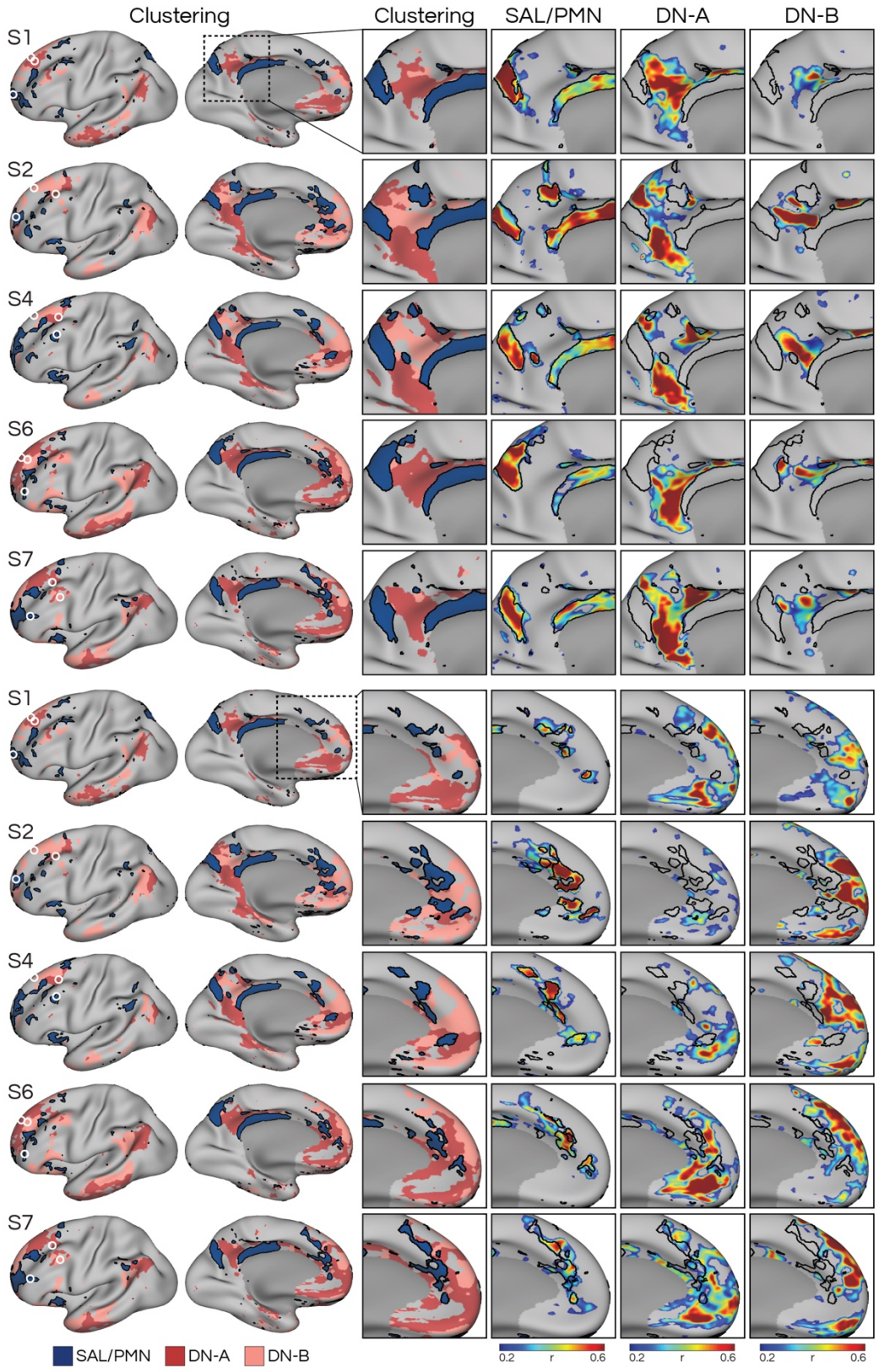

Supp. Fig. S6: Detailed anatomy of the salience/parietal memory network (SAL/PMN) reveals regions that are closely-knit with but distinct from networks within the canonical default network (DN) in additional individuals, Related to Fig. 1, 2, and 3. Figure formatted according to Supp. Fig. S5A. A representative individual S3 is shown in Supp. Fig. S5A.

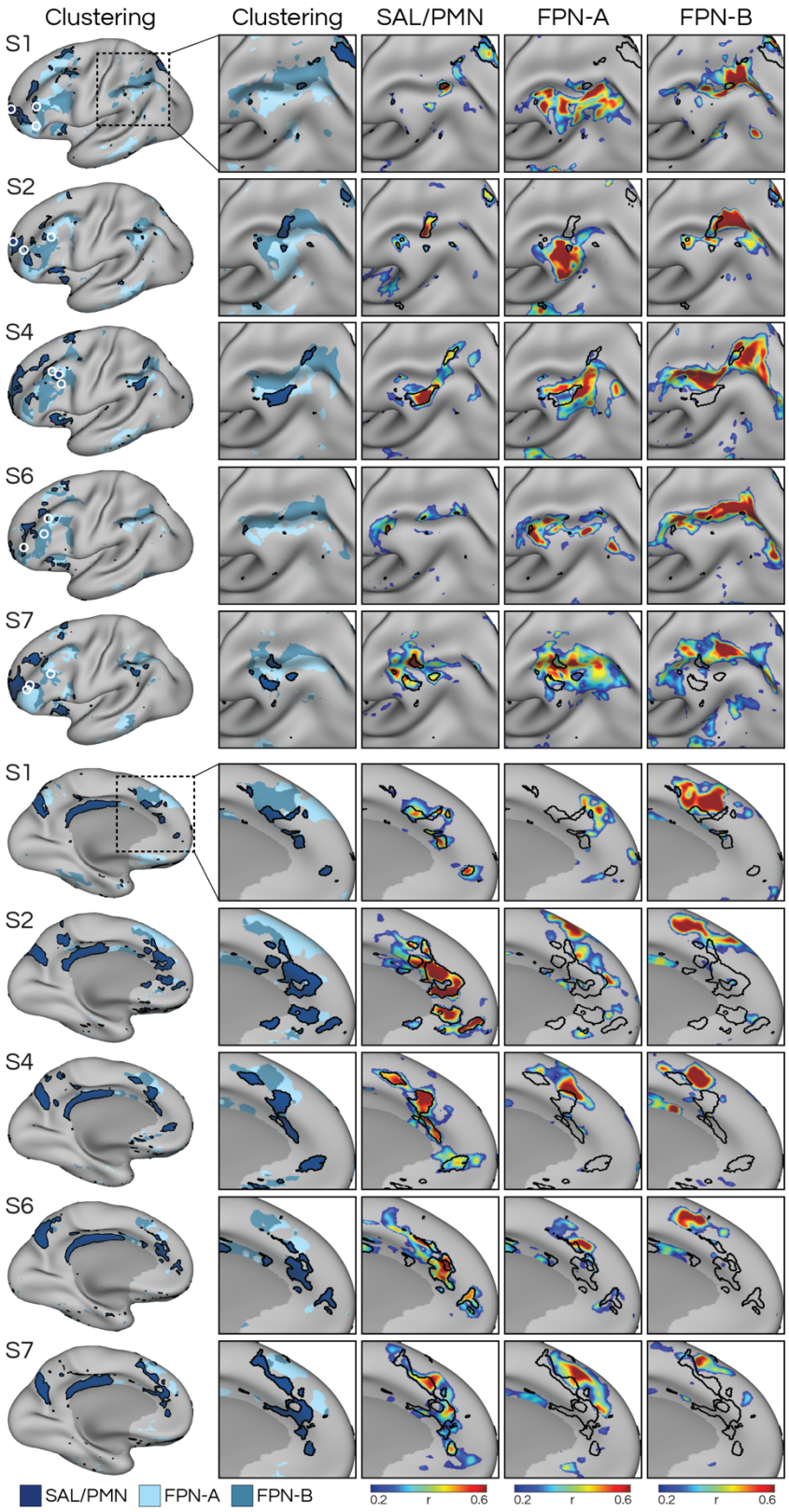

Supp. Fig. S7: Detailed anatomy of the salience/parietal memory network (SAL/PMN) reveals regions that are closely-knit with but distinct from networks within the canonical frontoparietal control network (FPN) in additional individuals, Related to Fig. 1, 2, and 3. Figure formatted according to Supp. Fig. S5B. A representative individual S3 is shown in Supp. Fig. S5B.

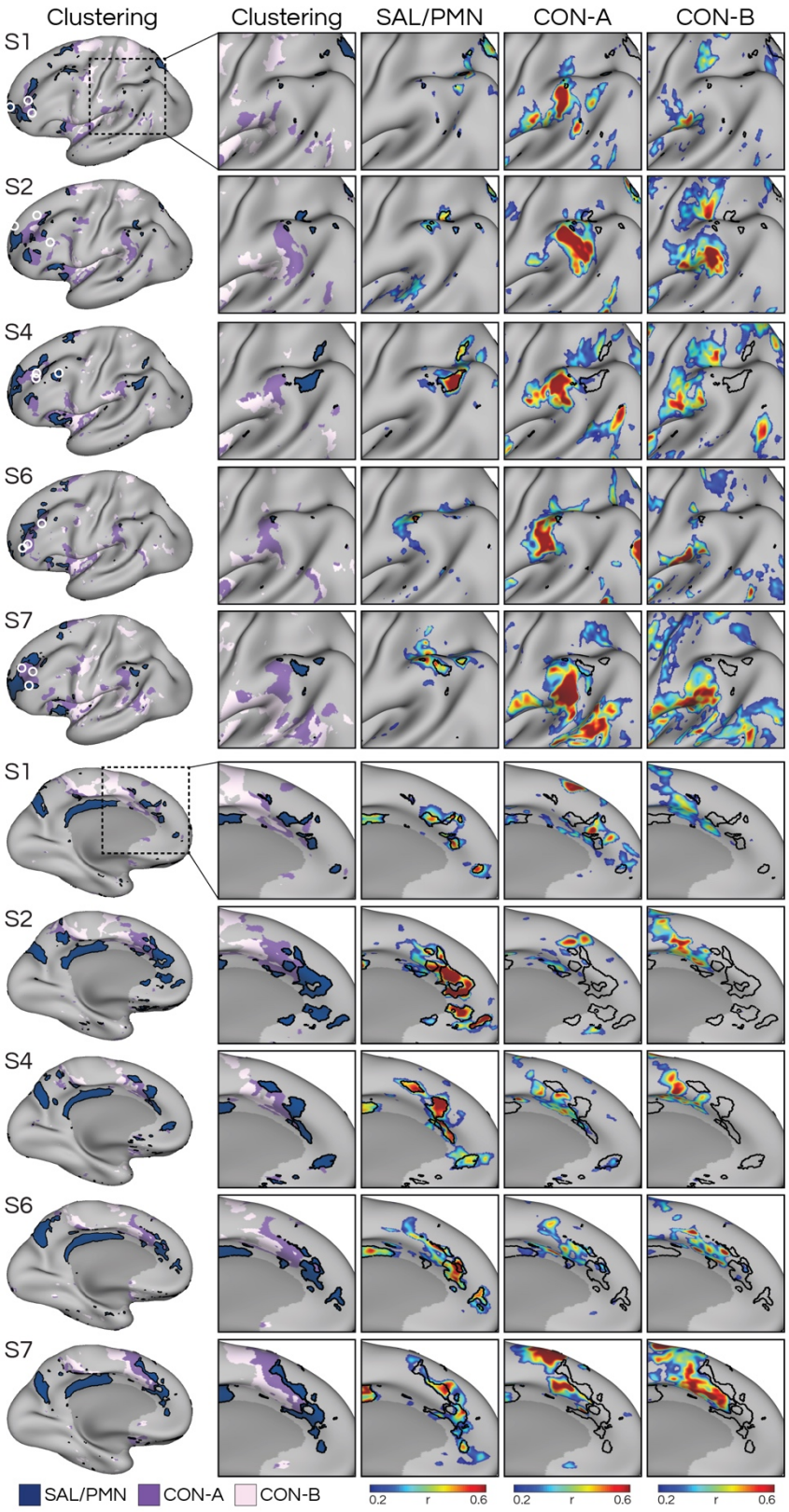

Supp. Fig. S8: Detailed anatomy of the salience/parietal memory network (SAL/PMN) reveals regions that are closely-knit with but distinct from the cingulo-opercular network (CON) in additional individuals, Related to Fig. 1, 2, and 3. Figure formatted according to Supp. Fig. S5C. A representative individual S3 is shown in Supp. Fig. S5C. See also targeted analysis of these networks in Fig. 6A.

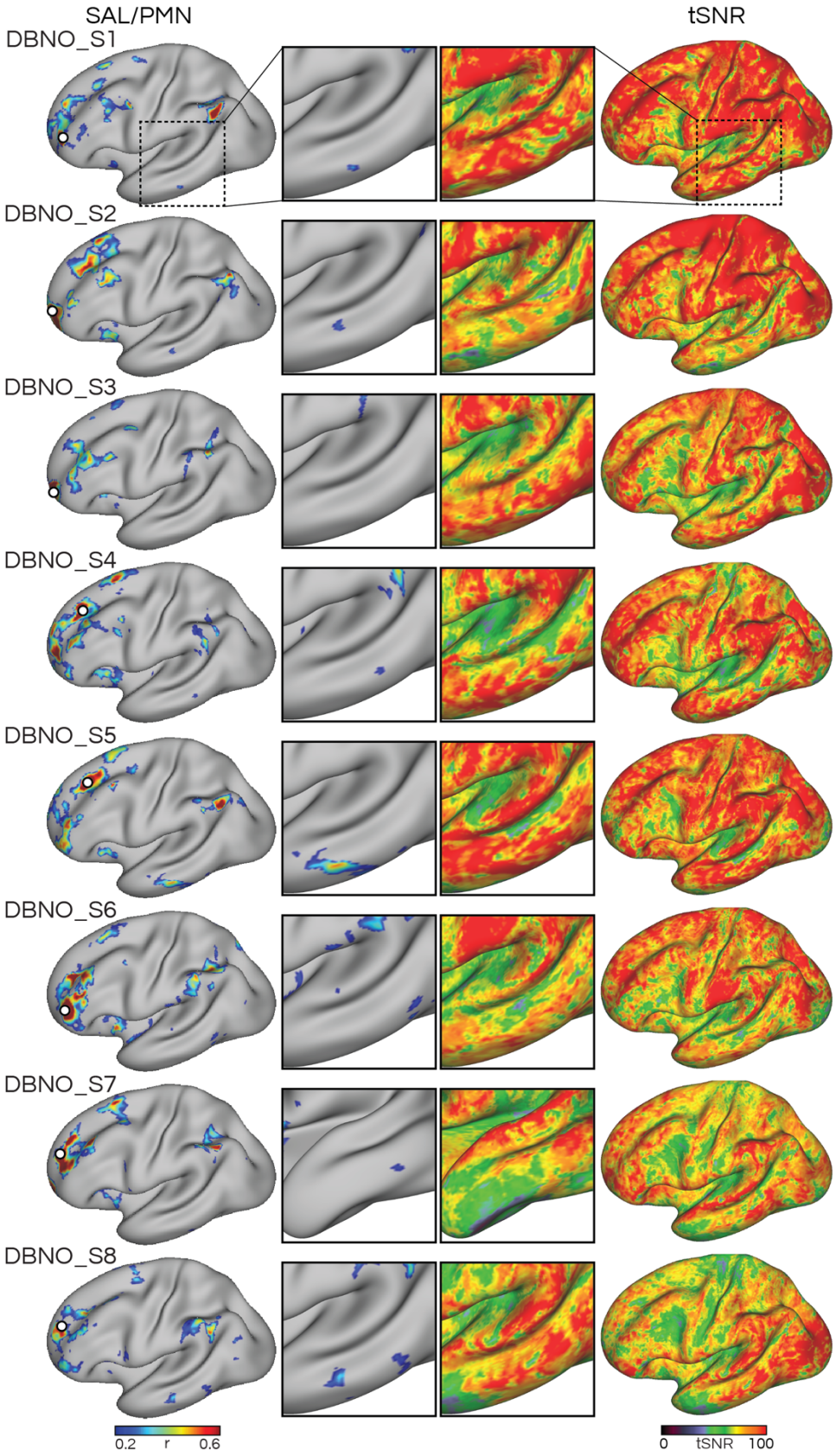

Supp. Fig. S9: Good data quality was achieved in the multi-echo 3T data (DBNO), with reduced dropout, Related to Fig. 5. Nonetheless, the seed-based map showed limited evidence for a SAL/PMN region in the lateral temporal cortex. The left columns show the functional connectivity map of the SAL/PMN defined using a seed-based approach (seeds shown as white circles), and the right columns show the temporal signal-

to-noise ratio (tSNR) maps for all eight individuals (rows). Insets show a zoom-in of the lateral temporal cortex. All subjects, except one (DBNO_S3) show a few vertices in the lateral temporal cortex that correlated above r > 0.2 with the rest of SAL/PMN, supporting that a lateral temporal region may exist here that is part of SAL/PMN. The inset of DBNO_S7 is rotated for better visualization of the region which was more ventral. Analysis of UK Biobank data containing 4,181 participants also suggested the presence of a PMN region here (see Fig. 4C). It is possible that despite improvements in tSNR, the 3T multi-echo data is of insufficient resolution or contrast to noise to reveal the SAL/PMN region robustly.

Supplementary Table S1: Extensive high-quality resting-state data were analyzed for each participant, and divided into discovery, replication, and triplication datasets, Related to STAR Methods. The table presents the number of good quality runs, a total amount of data included, and quality control metrics for the discovery, replication, and triplication datasets for each individual. The quality metrics include signal-to-noise ratio (tSNR), maximum absolute head motion (max motion), and maximum framewise displacement (max FD). The mean values are presented, with standard deviations in parentheses**.** Runs that fell below our quality control criteria were excluded from the full dataset, leading to the complete exclusion of 2 of the NSD subjects (S5 and S8).

	S1	S2	S3	S4	S6	S7
Discovery dataset						
# of runs	17	6	8	6	7	6
amount of data (min)	85	30	40	30	35	30
tSNR	165.14 (38.39)	134.52 (53.72)	157.24 (36.48)	141.65 (26.54)	99.19 (23.36)	157.58 (37.79)
max motion (mm)	0.43 (0.11)	0.74 (0.26)	0.48 (0.17)	0.67 (0.30)	0.68 (0.16)	0.54 (0.18)
max FD (mm)	0.26 (0.06)	0.38 (0.05)	0.26 (0.07)	0.22 (0.09)	0.18 (0.05)	0.15 (0.04)
Replication dataset						
# of runs	9		8	6	6	6
amount of data (min)	45		40	30	30	30
tSNR	147.71 (33.03)	—	159.79 (51.20)	153.77 (35.57)	108.33 (14.36)	178.97 (45.88)
max motion	0.36 (0.06)		0.59 (0.23)	0.62 (0.33)	0.64 (0.30)	0.61 (0.22)
max FD	0.22 (0.03)		0.28 (0.04)	0.19 (0.08)	0.14 (0.04)	0.15 (0.03)
Triplication dataset						
# of runs	9				6	6
amount of data (min)	45				30	30
tSNR	148.94 (27.47)	—	—	—	123.52 (35.30)	133.95 (33.50)
max motion	0.39 (0.14)				0.68 (0.25)	0.56 (0.21)
max FD	0.24 (0.05)				0.14 (0.07)	0.15 (0.05)

Supplementary Table S2: High quality resting-state data were analyzed in an independent 3T validation dataset (Detailed Brain Network Organization study or DBNO) that included eight participants, Related to STAR Methods. The table presents the number of runs included, total amount of data, and quality control metrics including signal-to-noise ratio (tSNR), maximum absolute head motion (max motion), and maximum framewise displacement (max FD), for the resting-state runs of the DBNO data. The mean values are shown, with standard deviations in parentheses.

	DBNO_01	DBNO_02	DBNO_03	DBNO_04	DBNO_05	DBNO_06	DBNO_07	DBNO_08
# of runs	8	8	8	8	10	7	7	7
amount of data (min)	56	56	56	56	70	49	49	49
tSNR	244.88 (32.30)	306.05 (29.55)	279.88 (28.56)	283.91 (54.29)	249.28 (32.77)	251.54 (47.55)	249.13 (31.17)	226.11 (34.55)
max motion (mm)	0.40 (0.29)	0.56 (0.21)	0.71 (0.46)	0.57 (0.29)	0.72 (0.33)	0.85 (0.28)	0.35 (0.20)	0.74 (0.36)
max FD (mm)	0.11 (0.04)	0.10 (0.03)	0.13 (0.07)	0.16 (0.04)	0.18 (0.05)	0.17 (0.03)	0.14 (0.09)	0.18 (0.03)